

Dear, Editor Ran Feng,

We have carefully revised and edited the manuscript entitled “Late Miocene-Pliocene climate evolution recorded by the red clay covered on the Xiaoshuizi planation surface, NE Tibetan Plateau” based on your valuable comments and suggestions. This time, we mainly revised the discussion of possible mechanisms for palaeo-EASM expansion during early Pliocene. Many thanks for spending so much time to review our manuscript. Wish you and yours have a happy Spring Festival in advance.

Judging by previous reviews, I lean towards trusting your geochemical and sedimentary analyses. However, I do have concerns about your discussion. I am worried that the discussion of mechanisms accounting for EASM expansion during early Pliocene was built upon misunderstanding of early Pliocene tropical SST records. The records cited in your discussion did not cover late Miocene, and hence should not be used to argue for expansion of monsoon starting from early Pliocene. The long records from western tropical Pacific actually suggest similar and warmer than present-day SSTs for both early Pliocene and late Miocene.

I recommend rewrite and shorten the discussion. Please stick with interpretations from sedimentary and geochemical features to monsoonal climate. The discussion of mechanisms reads very weak, and as shown above, erroneous at various places.

Our response: Many thanks for your valuable suggestions. We remove the statement of lines 488-498 and lines 546-570.

See details in the below:

Line 566 to 572, Brierley et al., 2009; Fedorov et al., 2013 did not suggest that equatorial SSTs remain stable or cooled. Instead, Brierley et al. suggests that warm pool was expanded during the early to mid-Pliocene. Zhang et al., (2014, science) actually suggests that western tropical Pacific was significantly warmer during the late Miocene and early Pliocene. The argument from line 566 and 575 is based on misunderstanding of published literatures.

Our response: We would remove this part.

Line 572 to line 575, the cited studies provide no theoretical basis on how the northern high latitude warming would affect ITCZ position. This argument again has no support.

Our response: We modify the statement as “On the other hand, the unusually warm Arctic and the West Antarctic ice-sheet expansion by 6–5 Ma (Zachos et al., 2001, 2008) steepened interhemispheric thermal gradient and could further cause the thermal equator to move northward (Chiang and Friedman, 2012; Broecker and Putnam, 2013). This facilitated the northwestward expansion of the palaeo-EASM, which is also proposed as the driving mechanism for northwestward migration of the monsoon rain belt for the warm Holocene (Yang et al., 2015).”

Line 582 to 584, again, misinterpretation of Brierley et al and Fedorov et al. Notice that the tropical Pacific records discussed in these papers DO NOT cover late Miocene for the most part. You CANNOT cite them to highlight the uniqueness of early Pliocene. In fact, based on

Zhang et al., 2012, the western tropical Pacific during late Miocene is not that different from early Pliocene.

Our response: We remove the statement.

Thanks for taking time to revise the manuscript! I am looking forward to your submission!

Other modifications

#1: In lines 40-42, the statement of “the poleward expansion of the tropical warm pool into subtropical regions, and the freshening of the subtropical Pacific” is removed.

#2: The statement of lines 488-498 is removed.

#3: Lines 533-536, the statement of “The warming of the northern high latitude region led to increases in summer temperature in the mid-latitudes of Eurasia. However, equatorial SSTs remained stable or cooled slightly (Brierley et al., 2009; Fedorov et al., 2013), and thus the land-ocean thermal contrast was intensified. Furthermore,” is modified to “Furthermore, a decrease in the input of ice-rafted debris to the sediments of the subarctic northwest Pacific was synchronous with the expansion of the palaeo-EASM during the early Pliocene (Fig. 6). The warming of the Northern Hemisphere and”.

#4: In line 537, “also” is removed.

#5: In line 546-548 “and small meridional heat gradient in the Northern Hemisphere pushed the Intertropical Convergence Zone northwards (Chang et al., 2013; Sun et al., 2015), which weakened the westerly circulation and thus facilitated the northwestward expansion of the palaeo-EASM” is modified to “and West Antarctic ice-sheet expansion by 6–5 Ma (Zachos et al., 2001, 2008) steepened interhemispheric thermal gradient and could further cause the thermal equator to move northward (Chiang and Friedman, 2012; Broecker and Putnam, 2013). This facilitated the northwestward expansion of the palaeo-EASM which is also proposed as the driving mechanism for northwestward migration of the monsoon rain belt for the warm Holocene (Yang et al., 2015).”

#6: The statement of lines 549-570 is removed.

#7: In line 571, “In conclusion” is modified to “Therefore”.

#8: In line 572-574, “accompanied by the vast poleward expansion of the tropical warm pool into subtropical regions and the freshening of the subtropical Pacific,” is modified to “in response to the closure of the Panamanian Seaway”.

#9: In line 581, “and SSTs of the low latitude Pacific Ocean” is removed.

#10: In lines 595-597, “the vast poleward expansion of the tropical warm pool into subtropical regions, and the freshening of the subtropical Pacific,” is removed.

#11: References of line 635, line 698 and line 702 are removed and “Broecker, W.S., Putnam A.E.: Hydrologic impacts of past shifts of Earth’s thermal equator offer insight into those to be produced by fossil fuel CO₂. Proc Natl Acad Sci USA 110(42):16710–16715, 2013. Chiang J. C. H., Friedman A. R.: Tropical cooling, interhemispheric thermal gradients, and tropical climate change. Annu Rev Earth Planet Sci 40(1):383–412, 2012. Yang, S.L., Ding, Z.L., Li, Y.Y., Wang, X., Jiang, W.Y., Huang, X.F.: Warming-induced northwestward migration of the East Asian monsoon rain

belt from the Last Glacial Maximum to the mid-Holocene. Proc. Natl. Acad. Sci. USA 112, 13178–13183, 2015. Zachos, J.C., Dickens, G.R., Zeebe, R.E., 2008. An early Cenozoic perspective on green-house warming and carbon-cycle dynamics. Nature.451, 279–283” are added.

#12: Fig 6 h and i are removed.

Hopefully the revised version is now satisfactory for publication in *Climate of the Past*.

Best regards,

Jijun Li

1 **Late Miocene-Pliocene climate evolution recorded by the red clay covered on the**
2 **Xiaoshuizi planation surface, NE Tibetan Plateau**

3
4 Xiaomiao Li¹, Tingjiang Peng¹, Zhenhua Ma¹, Meng Li¹, Zhantao Feng¹, Benhong Guo¹, Hao Yu¹, Xiyan
5 Ye¹, Zhengchuang Hui¹, Chunhui Song², Jijun Li^{1,3}

6
7 1. MOE Key Laboratory of Western China's Environmental Systems, College of Earth and Environmental
8 Sciences, Lanzhou University, Lanzhou 730000, China

9 2. School of Earth Sciences, Key Laboratory of Western China's Mineral Resources of Gansu Province,
10 Lanzhou University, Lanzhou 730000, China

11 3. College of Geography Science, Nanjing Normal University, Nanjing 210023, China

12
13
14
15
16
17
18 _____
19 *Corresponding author: Key Laboratory of Western China's Environmental Systems
20 (Ministry of Education), College of Earth and Environmental Science, Lanzhou University,
21 Lanzhou 730000, China; *E-mail address*: lijj@lzu.edu.cn (J.J. Li), *Fax*: +86-931-891-2724;
22 *Tel.*: +86-931-891-2724

23 Abstract

24 The Pliocene climate and its driving mechanisms have attracted substantial scientific
25 interest because of their potential as an analog for near-future climates. The late Miocene-
26 Pliocene red clay sequence of the main Chinese Loess Plateau (CLP) has been widely used to
27 reconstruct the history of interior Asian aridification and the Asian monsoon. However, red
28 clay sequences deposited on the planation surface of the Tibetan Plateau (TP) are rare. A
29 continuous red clay sequence was recently discovered on the uplifted Xiaoshuizi (XSZ)
30 planation surface in the Maxian Mountains, northeastern (NE) TP. In this study, we analyzed
31 multiple climatic proxies from the XSZ red clay sequence with the aim of reconstructing the
32 late Miocene-early Pliocene climate history of the NE TP and to assess regional climatic
33 differences between the central and western CLP. Our results demonstrate the occurrence of
34 minimal weathering and pedogenesis during the late Miocene, which indicates that the
35 climate was arid. We speculate that precipitation delivered by the palaeo- East Asian Summer
36 Monsoon (EASM) was limited during this period, and that the intensification of the
37 westerlies circulation resulted in arid conditions in the study region. Subsequently, enhanced
38 weathering and pedogenesis occurred intermittently during 4.7-3.9 Ma, which attests to an
39 increase in effective moisture. We ascribe the arid-humid climatic transition near ~4.7 Ma to
40 the expansion of the palaeo-EASM. ~~The warming of the high northern latitudes~~Increasing
41 ~~Arctic temperatures, the poleward expansion of the tropical warm pool into subtropical~~
42 ~~regions, and the freshening of the subtropical Pacific~~ in response to the closure of the
43 Panamanian Seaway, may have been responsible for the thermodynamical enhancement of
44 the palaeo-EASM system, which permitted more moisture to be transported to the NE TP.

45 **Keywords:** Late Miocene-Pliocene; Xiaoshuizi Planation Surface; Red Clay; Palaeo-EASM;
46 Westerly Circulation

47

48 **1. Introduction**

49 The Pliocene, including the Zanclean (5.33-3.60 Ma) and Piacenzian (3.60-2.58 Ma)
50 stages, is one of the most intensively studied intervals of the pre-Quaternary in climate
51 change research. The Zanclean climate was generally warm and wet and is often used as an
52 analogue for near-future climate conditions in terms of carbon dioxide levels, ranging from
53 280-415 ppm ([Tripathi et al., 2009](#); [Pagani et al., 2010](#)), and comparable temperatures in the
54 tropical region ([Herbert et al., 2010, 2016](#)). On the other hand, the Zanclean was markedly
55 different from today, although several critical changes in thermohaline and atmospheric
56 circulation towards modern conditions were occurring ([Haug et al., 2005](#); [Lawrence et al.,](#)
57 [2006](#); [Chaisson and Ravelo, 2000](#)). For example, the early-Pliocene global mean
58 temperature was approximately 4 °C warmer ([Brierley and Fedorov, 2010](#)), and the sea
59 levels are estimated to have been ~25 m higher, than today ([Dowsett et al., 2010](#)).

60 Temperatures at high northern latitudes were considerably higher and therefore continental
61 glaciers were almost absent from the Northern Hemisphere ([Ballantyne et al., 2010](#); [Dowsett](#)
62 [et al., 2010](#)). The zonal and meridional sea surface temperature gradients in the Northern
63 Hemisphere were weak but gradually became more intensified, changing towards the
64 modern state which has a much more pronounced spatial temperature contrast ([Fedorov et](#)
65 [al., 2013](#); [Brierley et al., 2009, 2010](#)). The low meridional surface temperature gradient

66 resulted in weaker meridional circulation during this interval (Fedorov et al., 2013; Brierley
67 et al., 2009), and the minor east-west sea surface temperature contrast in the tropical Pacific
68 during this interval is believed to have given rise to a permanent El Nino Southern
69 Oscillation (Lawrence et al., 2006); however, whether permanent El Nino-like conditions
70 were sustained during the Pliocene is controversial (Wara et al., 2005; Watanabe et al., 2011;
71 Zhang et al., 2014). In addition, the episodic uplift of the TP (Li et al., 2015; Zheng et al.,
72 2000; Fang et al., 2005a, 2005b) and gradual closure of the Panama Seaway (Keigwin et
73 al., 1978; O’Dea et al., 2016) were underway. The former had a substantial climatic impact
74 (An et al., 2001; Ding et al., 2001; Liu et al., 2014) and the latter resulted in the
75 reorganization of the global thermohaline circulation system (Haug et al., 1998, 2001).
76 These features imply a spatial change in the organization of the global climate system from
77 the early Pliocene to the present. In this context, it is important to characterize the response
78 of regional climates to these major global climatic and tectonic changes.

79 East Asia is one of the key regions for studying the aridification of the Asian interior
80 and the Asian monsoon evolution, which are tightly linked to the uplift of the TP, regional
81 climate change, and the evolution of global temperature and ice volume (An et al., 2001;
82 Ding et al., 2001; Li et al., 2008; Clift et al., 2008; Nie et al., 2014; Ao et al., 2016; Sun et
83 al., 2006a, 2017; Chang et al., 2013; Liu et al., 2014). Previous research has revealed that
84 red clay was widely deposited across the CLP since the late Miocene, indicating that Asian
85 aridification was enhanced (Guo et al., 2001; Song et al., 2007; An et al., 2014; Ao et al.,
86 2016; Li et al., 2017). In the eastern and central CLP, where the climate is dominated by the
87 East Asian Monsoon, palaeontological evidence, mineral magnetic parameters and

88 geochemical records from the red clay indicate dry climatic conditions during the late
89 Miocene but generally wet climatic conditions during the early Pliocene (Wang et al., 2006;
90 Guo et al., 2001; Wu et al., 2006; Song et al., 2007; Sun et al., 2010; An et al., 2014; Ao et
91 al., 2016). The most controversial climatic change occurred during the interval from 4.8-4.1
92 Ma, for which climate reconstructions using different proxies indicate conflicting palaeo-
93 environmental trends. For example, field observations and pollen records indicate an
94 intensified summer monsoon intensity, but low magnetic susceptibility values are more
95 consistent with arid rather than wet climatic conditions (Ding et al., 2001; Ma et al., 2005;
96 Song et al., 2007; Sun et al., 2010). It is thought that dissolution of ferrimagnetic minerals
97 and iron reduction resulting from high precipitation significantly affected the climatic
98 significance of magnetic susceptibility records during this period (Ding et al., 2001). In
99 addition to the East Asian Monsoon, the westerlies also had an impact on the climate of East
100 Asia; however, the patterns of climate change in the westerlies-dominated regions were
101 different from the eastern and central CLP during the early Pliocene. Geochemical,
102 stratigraphic and pollen evidence from the Qaidam and Tarim basins has demonstrated that
103 aridification intensified since the early Pliocene (Fang et al., 2008; Sun et al., 2006a, 2017;
104 Chang et al., 2013; Liu et al., 2014). Although the general climatic trends of the main CLP
105 and central Asia during this period are well recorded, palaeoclimatic changes in the NE TP,
106 which is at the junction of the zones of westerlies and monsoonal influences, remain unclear.
107 Therefore, determining the climatic conditions of the NE TP during the early Pliocene not
108 only improves our understanding of the pattern of regional climate change, but it may also
109 provide insights into the responses of the palaeo-EASM and the westerlies to TP uplift and

110 changes in the global climate system.

111 A continuous red clay sequence was recently discovered on the uplifted XSZ planation
112 surface in the NE TP and has been dated via high-resolution magnetostratigraphy (Li et al.,
113 2017). Due to its specific geographical location, the XSZ red clay provides the opportunity
114 to reveal the late Miocene-early Pliocene climate history of the NE TP and to determine the
115 climatic differences between the central and western CLP. In this study, we measured
116 multiple climatic proxies from the late Miocene-Pliocene XSZ red clay core. Our aims were
117 to construct a detailed record of precipitation, chemical weathering and pedogenesis during
118 6.7-3.6 Ma; and to determine the pattern of regional climate evolution and its possible causal
119 mechanisms.

120

121 **2. Regional background**

122 The XSZ planation surface is located in Yuzhong County in the western Chinese Loess
123 Plateau (Fig. 1). The main XSZ planation surface is at an altitude of 2800 m in the Maxian
124 Mountains where it has truncated Precambrian gneiss. The Maxianshan are rejuvenated
125 mountains which protrude into the broad Longzhong Basin; they are located within a
126 climatically sensitive zone because of the combined influences of the Asian Monsoon and the
127 northern branch of the mid-latitude westerly circulation system. The planation surface is
128 mantled by over 30 m of loess and over 40 m of red clay. Our previous bio-
129 magnetostratigraphic study demonstrates that the red clay sequence covering the XSZ
130 planation surface is dated to ~6.9-3.6 Ma (Li et al., 2017). Here, we use the XSZ drill core to
131 reconstruct and discuss the patterns of regional climate change during the Miocene-Pliocene.

132 The long, continuous well-dated record of the drill core is superior to that of the Shangyaotan
133 core analyzed in Li et al. (2017). Yuzhong County lies within the semi-arid temperate climate
134 zone at the junction of the eastern monsoon area, the arid area of northwest China, and the
135 cold region of the TP. The mean annual temperature during 1986-2016 was ~7.0 °C and the
136 annual precipitation was 260-550 mm; 80% of the precipitation is in summer and autumn
137 (data source: National Meteorological Information Center (<http://data.cma.cn/>) of the Chinese
138 Meteorological Administration). The spatial distribution of precipitation is uneven,
139 decreasing from south to north in Yuzhong County. Precipitation amount increases with
140 elevation at the rate of 27 mm per 100 m, attaining a maximum of 800 mm at the top of
141 Maxianshan.

142

143 **3. Material and methods**

144 The XSZ core (35.8115 °N, 103.8623 °E and 2758.1 m above sea level) is composed of
145 42 m of pure red clay and ~3 m of red clay and there is an increasing content of angular
146 gravel at the base (Fig. 1 b). The red clay interval is composed of brownish red and yellowish
147 clay layers (Fig. 2). The upper 20 m contains numerous horizontal carbonate nodule horizons
148 (Bk), most of which underlie brownish red soil layers (Bw) characterized by loam and
149 moderate medium angular blocky structure. There are also occasional carbonized plant root
150 channels, elliptical worm burrows and fossil snail shell fragments. Fe-Mn stains are more
151 frequent in the brownish layers than in the yellowish layers, which is also the case for the
152 carbonized root channels. The red clay across the XSZ planation surface is similar to that of
153 typical eolian red clay in the CLP; both are characterized by numerous carbonate nodule-rich

154 horizons (Fig. 2 b).

155 Samples for grain-size, carbonate content and magnetic susceptibility measurements
156 were taken at 5-cm intervals, and samples for geochemical analysis were collected at 25-cm
157 intervals. Samples for grain-size measurements were pre-treated with 10% H₂O₂ to remove
158 organic material, with 10% HCl to remove carbonates, and with 0.05 mol/L of (NaPO₃)₆ for
159 dispersion. They were then measured with a Malvern Mastersizer 2000 grain-size analyzer
160 with a detection range of 0.02-2000 μm. Magnetic susceptibility was measured using a
161 Bartington Instruments MS2 meter and MS2B dual-frequency sensor at two frequencies (470
162 Hz and 4700 Hz, designated χ_{lf} and χ_{hf} , respectively). Three measurements were made at each
163 frequency and the final results were averaged. The frequency-dependent magnetic
164 susceptibility (χ_{fd}) was calculated as $\chi_{lf} - \chi_{hf}$. Chemical composition was measured via X-ray
165 fluorescence using a Panalytical Magix PW2403 with an error of 0.1%-0.3%. The sample
166 preparation procedure for XRF analysis was as follows: Bulk samples were heated to 35°C
167 for 7 days and then ground with an agate mortar to pass a 75-μm sieve; ~4 g of powdered
168 sample was then pressed into a pellet with a borate coating using a semiautomatic oil-
169 hydraulic laboratory press (model YYJ-40). All the measurements were conducted at the
170 MOE Key Laboratory of Western China's Environmental Systems, Lanzhou University.
171 Silicate-bound CaO (CaO*) can be estimated, in principle, by the equation: CaO*(mol) =
172 CaO(mol) – CO₂(calcite mol) – 0.5 CO₂(dolomite mol) – 10/3 P₂O₅(apatite mol) (Fedo et al.,
173 1995). It is generally calculated based on the assumption that all the P₂O₅ is associated with
174 apatite and all the inorganic carbon is associated with carbonates. Thus, the CaO* of the XSZ
175 red clay was calculated using the following equivalent equation:

176
$$CaO^*(mol) = CaO(mol) - CaCO_3(mol) - \frac{10}{3} * \frac{P_2O_5}{M(P_2O_5)}$$

177 The carbonate content was measured with a calcimeter using the volumetric method of
178 Avery and Bascomb (1974) in the Key Laboratory of Mineral Resources in Western China
179 (Gansu Province), Lanzhou University.

180 We used the coefficient of variation (CV) to measure the variability of the records: the
181 higher the CV, the more variable the record. The CV is defined as:

$$CV=100* \frac{\text{Standard deviation}}{\text{Mean}}$$

182 Each sample age was estimated using linear interpolation to derive absolute ages,
183 constrained by our previous magnetostratigraphic study (Fig. 1). The average temporal
184 resolution of the records is 3.8 kyr. Some 80 % of the sequence has a sampling resolution of 4
185 kyr or less. After interpolation to a 3-kyr sampling interval, we performed spectral analysis
186 on detrended records of carbonate content and χ_{pedo} using Redfit, based on the Lomb-Scargle
187 Fourier transform combined with a Welch-Overlapped Segment averaging procedure. We
188 applied Gaussian band-pass filters at frequencies of 0.09090-0.01111, 0.02174-0.02778 and
189 0.04167-0.05556 kyr⁻¹ to extract oscillations associated with the 100-kyr, 41-kyr and 21-kyr
190 periodicities, respectively. The significance of the correlations is based on a two-tailed test.

191 **4. Results**

192 Profiles of the various environmental proxies are illustrated in Figure 3. Notably, there is
193 evidence for a relatively wet interval from ~16-5 m (4.7-3.9 Ma) which is reflected in the
194 high-frequency occurrence of Bw horizons with a low carbonate content (< 8 %) and
195 intermittent enhancement of magnetic susceptibility. There is a large contrast in carbonate
196 content between Bw and Bk horizons, which corresponds to variations in elemental contents.

197 The Bk horizons, with a higher carbonate content, consist of carbonate nodule layers
198 underlying leached zones in the field indicate the substantial translocation of carbonate
199 minerals from Bw horizons to Bk horizons due to greater rainfall (He et al., 2013). In
200 addition, the CV of most of the records is greater during this interval than in other intervals
201 (Table 1). These various forms of evidence suggest that the climate became more humid and
202 variable during 4.7-3.9 Ma. The characteristics of the individual proxy records are described
203 in detail below.

204 **Carbonate content**

205 The carbonate content of the entire core fluctuates from 1.6-39.2% with an average of
206 15.9 %. From 42-16 m, the average carbonate content is high (17.1%) and the carbonate
207 content decreases upwards. The contrast in the carbonate content between the Bw and Bk
208 horizons is generally low; for the Bw horizons, the carbonate content is ~12% and values <8%
209 are rare. Bk horizons, with a carbonate content of around or above 21%, are frequent (Fig. 3).
210 From 16-5 m, there are fluctuations in carbonate content of large amplitude (1.6-39.1%) but
211 the average value is low (13.3%). Bw-Bk horizons are frequent; the Bw horizons have a
212 carbonate content of <8%, while that of the Bk horizons is >21%. From 5-0 m, the average
213 carbonate content increases to 15.5%; Bw horizons with a carbonate content <8% is absent,
214 and the carbonate content contrast between the Bw and Bk horizons is low.

215 **Element geochemistry**

216 K_2O ranges from 1.9-3.7% with an average of 2.8%; Na_2O ranges from 0.14-1.54% with
217 an average of 1.2%; Rb ranges from 74-134 ppm with an average of 106.2 ppm; and Sr
218 ranges from 141-281 ppm with an average of 212.8 ppm. The variations in CaO exhibit the

219 same trend as carbonate content with high values in Bk horizons and low values in Bw
220 horizons. The variations in Rb and K₂O are synchronous and roughly inverse to those of CaO.
221 The changes of Sr show some similarity with magnetic susceptibility prior to 4.7 Ma but with
222 CaO after 4.7 Ma. Reference to Table 2 shows that CaO is positively correlated with CaCO₃
223 and Sr, and negatively correlated with the other elements. From 16-5 m, CaO and Sr exhibit
224 low values in Bw horizons and high values in Bk horizons, while the opposite is the case for
225 K₂O and Rb. Finally, from 16-5 m, the amplitudes of the fluctuations in CaO, K₂O, Sr and Rb
226 are greater than in the other intervals.

227 **Magnetic susceptibility**

228 The variations of χ_{hf} , χ_{lf} and χ_{fd} are synchronous. χ_{hf} ranges from $9.6-53.9 \times 10^{-8} \text{ m}^3/\text{kg}$
229 with an average of $21.8 \times 10^{-8} \text{ m}^3/\text{kg}$; χ_{lf} ranges from $11.4-59.0 \times 10^{-8} \text{ m}^3/\text{kg}$ with an average of
230 $23.1 \times 10^{-8} \text{ m}^3/\text{kg}$; and χ_{fd} ranges from $0-4.7 \times 10^{-8} \text{ m}^3/\text{kg}$ with an average of $1.2 \times 10^{-8} \text{ m}^3/\text{kg}$.
231 From 42-16 m, the three magnetic parameters are relatively low and uniform. χ_{hf} ranges from
232 $9.6-33.3 \times 10^{-8} \text{ m}^3/\text{kg}$ with an average of $19.4 \times 10^{-8} \text{ m}^3/\text{kg}$; χ_{lf} ranges from $11.4-36.1 \times 10^{-8} \text{ m}^3/\text{kg}$
233 with an average of $20.3 \times 10^{-8} \text{ m}^3/\text{kg}$; and χ_{fd} ranges from $0-2.8 \times 10^{-8} \text{ m}^3/\text{kg}$ with an average of
234 $1.0 \times 10^{-8} \text{ m}^3/\text{kg}$. From 16-5 m, the values of the three parameters, together with their
235 amplitudes of variation, are high. χ_{hf} ranges from $13.8-53.9 \times 10^{-8} \text{ m}^3/\text{kg}$ with an average of
236 $27.4 \times 10^{-8} \text{ m}^3/\text{kg}$; χ_{lf} ranges from $14.2-59.0 \times 10^{-8} \text{ m}^3/\text{kg}$ with an average of $29.0 \times 10^{-8} \text{ m}^3/\text{kg}$;
237 and χ_{fd} ranges from $0-4.7 \times 10^{-8} \text{ m}^3/\text{kg}$ with an average of $1.6 \times 10^{-8} \text{ m}^3/\text{kg}$. Within the intervals
238 of 16-15 m, 13-11 m and 7-5 m, the values of the three parameters increase substantially.
239 From 5-0 m, both the values and amplitudes of variation of the three parameters decrease. χ_{hf}
240 ranges from $12.8-32.9 \times 10^{-8} \text{ m}^3/\text{kg}$ with an average of $22.0 \times 10^{-8} \text{ m}^3/\text{kg}$; χ_{lf} ranges from 13.6-

241 $34.6 \times 10^{-8} \text{ m}^3/\text{kg}$ with an average of $22.9 \times 10^{-8} \text{ m}^3/\text{kg}$; and χ_{fd} ranges from $0-2.5 \times 10^{-8} \text{ m}^3/\text{kg}$
242 with an average of $1 \times 10^{-8} \text{ m}^3/\text{kg}$. Overall, the fluctuations in magnetic susceptibility are
243 substantially different to those of carbonate content which indicates that the enhancement of
244 magnetic susceptibility was not caused by carbonate leaching.

245 **Grain size**

246 The clay content ($<2 \mu\text{m}$) ranges from 3.8-13.5% with an average of 8.17%; and the >40
247 μm content ranges from 0.7-13.9% with an average of 6%. The fluctuations in clay content
248 are minor, except for maxima at about 15 m, 12 m and 6 m, which correspond to peaks in
249 magnetic susceptibility (Fig. 3). The coarse silt component ($>40 \mu\text{m}$), mainly carried by the
250 East Asian winter monsoon, exhibits a different trend to that of the clay content. In addition,
251 from 21-5 m the fluctuations in the $>40 \mu\text{m}$ fraction are roughly the inverse to those of
252 magnetic susceptibility. From 42-21 m, the variation of the $>40 \mu\text{m}$ fraction is characterized
253 by low values and high-frequency fluctuations, whereas above 21 m it exhibits high values
254 and fluctuations of lower frequency.

255

256 **5. Discussion**

257 **5.1 Palaeoenvironmental interpretation of the proxies**

258 The carbonate content of aeolian sediments can be readily remobilized and deposited in
259 responses to changes in precipitation and evaporation intensity and thus is sensitive to
260 changing climatic conditions. Previous studies demonstrated that the carbonate content of
261 loess-red clay sequences of the CLP varies with precipitation (Fang et al., 1999; Sun et al.,
262 2010). The carbonate is mainly derived from a mixture of airborne dusts (Fang et al., 1999).

263 Soil micromorphological evidence from the Lanzhou loess demonstrates that the carbonate
264 grains in loess are little altered, whereas those in the palaeosols have undergone a reduction
265 in size as a result of leaching and reprecipitation as secondary carbonate in the lower Bk
266 horizons (Fang et al., 1994, 1999). Furthermore, seasonal alternations between wet and dry
267 conditions are thought to be a key factor driving carbonate dissolution and reprecipitation
268 (Sun et al., 2010). Thus, changes in carbonate content are generally controlled by the
269 effective precipitation. When effective precipitation is high, carbonate leaching increases, and
270 vice versa. Thus, the carbonate content is an effective proxy for characterizing wet-dry
271 oscillations as well as summer monsoon evolution (Fang et al., 1999; Sun et al., 2010).

272 Chemical weathering intensity is generally evaluated by the ratio of mobile (e.g. K, Ca,
273 Sr and Na) to non-mobile elements (e.g. Al and Rb). In general, Sr shows analogous
274 geochemical behavior to Ca and is readily released into solution and mobilized in the course
275 of weathering; by contrast, Rb is relatively immobile under moderate weathering conditions
276 due to its strong adsorption to clay minerals (Nesbitt et al., 1980; Liu et al., 1993). Thus, the
277 Rb/Sr ratio potentially reflects chemical weathering intensity. However, Sr may substitute for
278 Ca in carbonates which may limit the environmental significance of the Rb/Sr ratio (Chang et
279 al., 2013; Buggle et al., 2011). The correlation between Sr and CaO* (silicate CaO) is
280 significant at the 99% confidence interval, while the correlation between Sr and CaCO₃ is not
281 significant. This means that the variations in Sr are determined by weathering intensity, and
282 therefore we speculate that in our samples the Rb/Sr ratio mainly reflects weathering intensity
283 (Fig. 4 c and d). In addition, the K₂O/Na₂O ratio is used to evaluate the secondary clay
284 content in loess and is also a measure of plagioclase weathering, avoiding biases due to

285 uncertainties in separating carbonate Ca from silicate Ca (Liu et al., 1993; Buggle et al.,
286 2011). Na₂O is mainly produced by plagioclase weathering and is easily lost during leaching
287 as precipitation increases. By contrast, K₂O (mainly produced by the weathering of potash
288 feldspar) is easily leached from primary minerals and is then absorbed by secondary clay
289 minerals with ongoing weathering (Yang et al., 2006; Liang et al., 2013). In the arid and
290 semi-arid regions of Asia, K₂O is enriched in palaeosols compared to loess horizons (Yang et
291 al., 2006). Thus, high K₂O/Na₂O ratios are indicative of intense chemical weathering.

292 In the red clay-loess sequence of the CLP, magnetic parameters and the clay content are
293 well correlated and thus are regarded as proxies of EASM strength (Liu et al., 2004). Aeolian
294 particles usually have two distinct magnetic components, consisting of detrital and pedogenic
295 material, respectively (Liu et al., 2004). χ_{lf} can reflect the combined susceptibility of both
296 components, but changes in χ_{lf} are mainly affected by changes in the concentration of
297 pedogenic magnetic grains (Liu et al., 2004). The grain-size distribution of pedogenic
298 particles within the superparamagnetic (SP) to single-domain (SD) size range has been shown
299 to be constant (Liu et al., 2004, 2005). Thus, χ_{fd} can be used detect SP minerals produced by
300 pedogenesis and therefore the correlation coefficient between χ_{lf} and χ_{fd} is a measure of the
301 contribution of such grains (<0.03 μm for magnetite) to the bulk susceptibility (Liu et al.,
302 2004; Xia et al., 2014). As shown in Figure 4a, χ_{lf} is positively correlated with χ_{fd} , which
303 means that the magnetic susceptibility of the XSZ red clay mainly reflects pedogenic
304 enhancement of the primary aeolian ferromagnetic content via the in-situ formation of fine-
305 grained ferrimagnetic material. Thus, the magnetic susceptibility primarily reflects pedogenic
306 intensity. Both the original and pedogenic magnetic signals can be separated using a simple

307 linear regression method (Liu et al., 2004; Xia et al., 2014), which we use to extract the
308 lithogenic (χ_0) and pedogenic magnetite/maghemite (χ_{pedo}) components. We found that
309 pedogenic magnetite/maghemite accounts for 11% of the susceptibility ($\chi_{\text{pedo}} = \chi_{\text{fd}} / 0.11$).

310 Pedogenesis results in enhanced secondary clay formation (Sun and Huang, 2006b);
311 however, not all of the clay particles are derived from in situ pedogenesis, but rather are
312 inherited from aeolian transport and deposition. Clay particles can adhere to coarser silt and
313 sand particles (Sun and Huang, 2006b). In the western CLP, the coarse silt ($>40 \mu\text{m}$) content
314 is regarded as a rough proxy of winter monsoon strength (Wang et al., 2002). Therefore, to
315 eliminate this signal from the primary clay particles, the $<2 \mu\text{m}/>40 \mu\text{m}$ ratio is proposed to
316 evaluate pedogenic intensity. Furthermore, the similarity of the variations of $<2 \mu\text{m}/>40 \mu\text{m}$
317 ratio and χ_{pedo} confirms that in this case $<2 \mu\text{m}/>40 \mu\text{m}$ ratio has the potential to evaluate the
318 pedogenic intensity (Fig. 6).

319 **5.2 Time- and frequency- domain analysis of carbonate content and χ_{pedo}**

320 The power spectral analyses of carbonate content and χ_{pedo} show different dominant
321 cycles (Fig. 5 a-b). In detail, χ_{pedo} is concentrated in the eccentricity (100 kyr), obliquity (41
322 kyr) and precession (21 kyr) bands and other periodicities (71 kyr and 27 kyr) are also
323 evident. By contrast, the carbonate signal is concentrated in the precession (21 kyr) and
324 obliquity (41 kyr) bands, but it also exhibits even more prominent periodicities of 56 kyr and
325 30 kyr. Furthermore, the fluctuations in CaCO_3 , weathering and pedogenesis indices agree
326 well with orbital eccentricity variations during 4.7-3.9 Ma (Fig. 5 d). Three orbital
327 periodicities were also detected at other sites in CLP, in the interval from the late Miocene to
328 the early Pliocene, confirming that changes in orbital parameters had a substantial impact of

329 the climate of the CLP (Han et al., 2011).

330 King (1996) proposed that non-orbital cycles may originate from harmonic effects or
331 interactions of the orbital cycles, while Lu (2004) ascribed them to unstable dust depositional
332 processes followed by varying degrees of pedogenesis in palaeosol units. In the XSZ section,
333 the deposition rate is low and uneven, which potentially resulted in the incomplete
334 preservation of the paleoclimatic signal, especially for the relatively short precession cycles.
335 In addition, pedogenesis and post-depositional compaction would also weaken the orbital
336 signals and produce spurious cycles. Moreover, the carbonate content at various depths is
337 affected by leaching which means that the record integrates soil polygenetic processes, thus
338 obscuring orbital forcing trends related to precipitation amount. Therefore, we speculate that
339 uneven and low deposition rates, combined with compaction and leaching processes, may
340 have weakened the orbital signals and may be responsible for the presence of non-orbital
341 cycles in the XSZ section.

342 To investigate the post-6.7 Ma frequency domain evolution of the climate signals in the
343 XSZ section, we filtered the carbonate content and χ_{pedo} time series at the periods of 100, 41,
344 and 21 kyr, using Gaussian band filters centered at frequencies of 0.01, 0.02439, and 0.04762,
345 respectively. We then compared the results with the equivalent filtered components of the
346 stacked deep-sea benthic oxygen isotope record. The results show that the fluctuations of the
347 three filtered components (especially the 41-kyr component) of both proxies change from a
348 low amplitude during 6.7-4.7 Ma to a relatively high amplitude during 4.7-3.9 Ma (Fig. 5 c).
349 The enhanced orbital-scale variability of the two proxies from 4.7-3.9 Ma implies increased
350 seasonality and wet-dry contrasts. This shift is not observed in the Earth orbital parameters

351 but is observed in the filtered 41-kyr component of the stacked deep-sea benthic oxygen
352 isotope record ($\delta^{18}\text{O}$). This may mean that the enhancement of wet-dry contrasts at the XSZ
353 site was not driven directly by changes in solar radiation intensity but rather was linked with
354 changes in ice volume or global temperature.

355 **5.3 Late Miocene-Pliocene climate history revealed by the Xiaoshuizi red clay**

356 **5.3.1 Multi-proxy evidence for a dry climate during the late Miocene**

357 We used the proxies of pedogenesis and chemical weathering to reconstruct the late
358 Miocene and early Pliocene climatic history of the Xiaoshuizi planation surface. During the
359 late Miocene, the relatively high carbonate values with minor fluctuations indicate that the
360 climate was dry, and low Rb/Sr and $\text{K}_2\text{O}/\text{Na}_2\text{O}$ ratios also support the occurrence of weak
361 chemical weathering. Notably, both the Rb/Sr and $\text{K}_2\text{O}/\text{Na}_2\text{O}$ ratios show opposite trends to
362 that of carbonate content, meaning that low effective precipitation resulted in weak chemical
363 weathering. Furthermore, the pedogenic proxies (χ_{pedo} and χ_{lf}), characterised by low values
364 with minor fluctuations, generally support the occurrence of weak pedogenesis under an arid
365 climate. Thus, the climate at the XSZ site was relatively arid during this interval, resulting in
366 weak chemical weathering and pedogenic intensity. However, there are several subtle
367 differences between the carbonate and pedogenic indexes. It is evident that the carbonate
368 content decreases with an increased amplitude of variation after 5.5 Ma, which is consistent
369 with the cycles of carbonate nodules within paleosol horizons observed in the field (Li et
370 al., 2017). It is possible that increased precipitation since 5.5 Ma induced eluviation and the
371 redeposition of carbonate. However, the pedogenic indexes indicate that the generally arid
372 climate was interrupted by two episodes of enhanced pedogenesis, at 5.85-5.7 Ma and 5.5-

373 5.35 Ma. The subtle differences may result from differences in the sensitivity of magnetic
374 susceptibility and carbonate content to precipitation variability when precipitation is low (Sun
375 et al., 2010). In addition, a coeval mollusk record from the western Liupanshan showed that
376 cold-aridiphilous species dominated, which also indicates that cold and dry climatic
377 conditions occurred in the western CLP during the late Miocene (Fig. 7 g).

378 Coeval pollen, mollusk and magnetic records from the central and eastern CLP also
379 indicate generally dry and cold climatic conditions (Wang et al., 2006; Wu et al., 2006; Nie et
380 al., 2014). However, the principal difference is that at the XSZ site, the arid climate was
381 relatively stable, while the climate of the central and eastern CLP was interrupted by several
382 humid stages. For example, two humid stages (6.2-5.8 Ma and 5.4-4.9 Ma) are recorded by
383 the magnetic susceptibility of the red clay in the central and eastern CLP but are absent in the
384 magnetic susceptibility record at the XSZ site (Fig. 7). Notably, the 41-kyr filtered
385 component of thermo-humidiphilous species from Dongwan was damped in the late Miocene
386 (Li et al., 2008). Similarly, the amplitude of the orbital periodicities, filtered from the XSZ
387 carbonate content and χ_{pedo} records, was obviously damped during 6.7-4.7 Ma. However, the
388 three periodicities in the Summer Monsoon index from the central CLP show no obvious
389 difference between the late Miocene and Pliocene, but only a slight reduction in variability
390 after 4.2 Ma (Sun et al., 2010). Therefore, we agree that a dry climate prevailed on the CLP
391 during the late Miocene; however, the difference was that the climate in the central and
392 eastern CLP fluctuated more substantially than was the case in the vicinity of the XSZ red
393 clay section.

394 The especially damped response of the wet-dry climatic oscillations in the western CLP

395 to obliquity forcing may indicate that the influence of the palaeo-EASM in the western CLP
396 was negligible. It is widely known that the summer monsoon intensity decreases from
397 southeast to northwest across the CLP. A regional climate model experiment demonstrated
398 that the modern East Asian Summer Monsoon was not fully established in the late Miocene
399 and had only a small impact on northern China (Tang et al., 2011). A weak palaeo-EASM
400 intensity from 7.0-4.8 Ma was revealed by hematite/goethite and smectite/kaolinite ratios at
401 ODP Site 1148 in the South China Sea (SCS) (Fig. 7 i and j). Therefore, we infer that the
402 palaeo-EASM was weak and had only a minor impact on the climate in the study region. In
403 addition, previous studies indicated that the red clay may have been transported by both low-
404 level northerly winds and the upper-level westerlies (Sun et al., 2004; Vandenberghe et al.,
405 2004) and thus the impact of the westerly circulation on the study region cannot be ignored.
406 Notably, the variation of the pedogenic proxies roughly parallels that of the stacked deep-sea
407 benthic foraminiferal oxygen isotope curve (Fig. 6), and that that χ_{pedo} has a positive
408 relationship with $\delta^{18}\text{O}$ (Fig. 4 e). This indicates that when the global temperature was low,
409 pedogenic intensity in the study area increased. It is unreasonable to conclude that
410 precipitation in the study area was dominated by the palaeo-EASM and thus we speculate that,
411 during the late Miocene, precipitation transported by the palaeo-EASM was limited and that
412 the westerly circulation probably dominated the regional climate.

413 The simultaneous reduction in amplitude of the 41-kyr filtered components from the
414 western CLP and the deep sea $\delta^{18}\text{O}$ record during the late Miocene likely indicates that the
415 dry climate was related to changes in global temperature and ice volume. A sustained cooling
416 occurred in both hemispheres during the late Miocene which culminated between 7 and 5.4

417 Ma (Herbert et al., 2016). $\delta^{18}\text{O}$ records from DSDP and ODP sites show an increase of $\sim 1.0\text{‰}$
418 during the late Miocene which resulted from the increased ice volume and the associated
419 decrease in global temperature (Zachos et al., 2001). In the Northern Hemisphere, transient
420 glaciations occurred when the cooling culminated (Herbert et al., 2016). Records from high-
421 latitude regions of the Northern Hemisphere indicate continuously decreasing temperatures
422 and increasing ice volume during the late Miocene (Jansen and Sjöholm, 1991; Mudie and
423 Helgason, 1983; Haug et al., 2005). During the Quaternary, a dry climate prevailed during
424 glacial periods when the global average temperature (especially in summer) was low. Cool
425 summers could result in a small land-sea thermal contrast which in turn weakened the palaeo-
426 EASM. Furthermore, the increased ice volume in the Northern Hemisphere resulted in an
427 increased meridional temperature gradient (Herbert et al., 2016), thus strengthening the
428 westerlies and driving them southwards. This would have prevented the northwestward
429 penetration of the Asian Summer Monsoon, which is also proposed as the driving mechanism
430 for a weak EASM in northern China during glacial periods (Sun et al., 2015). Thus, the
431 southward shift of the westerlies had a significant impact on the XSZ region. However,
432 moisture sources for the westerly air flow are distant from the CLP (Nie et al., 2014), and
433 only a relatively small amount of moisture was carried to the CLP, resulting in a dry and
434 stable climate in the XSZ region. In conclusion, global cooling and increasing ice volume in
435 the Northern Hemisphere contributed to the dry climatic conditions in the study region.

436 **5.3.2 Intermittently humid climate during the early Pliocene**

437 During the early Pliocene, the proxy evidence indicates that the previously arid climate
438 of the XSZ area became humid from ~ 4.7 Ma. The carbonate content was low on average but

439 with large fluctuations, indicating that the climate was generally humid with increased dry-
440 wet oscillations, especially during 4.7-3.9 Ma. Several eluvial-illuvial cycles are evident
441 during 4.7-3.9 Ma; the carbonate content in the eluvial horizons was less than 8%, whereas in
442 illuvial horizons it was >21% (Fig. 6). Research on the migration process of carbonate
443 indicate that a seasonally wet/dry climate is a key factor in driving carbonate dissolution and
444 reprecipitation, and strong seasonally-biased precipitation enhances the leaching process and
445 produces thick leached horizons (Rossinsky and Swart, 1993; Zhao, 1995, 1998). The
446 occurrence of high-frequency cycles of carbonate eluviation-redeposition indicates that
447 seasonal precipitation increased during this interval. Furthermore, the variations of Rb/Sr and
448 K_2O/Na_2O ratios are very similar to those of carbonate content, which suggests that
449 weathering intensity was related to precipitation amount. Generally, high values of the $<2 \mu m$
450 / $>40 \mu m$ ratio, χ_{pedo} and χ_{lf} correspond to large contrasts in carbonate content between eluvial
451 and illuvial horizons; thus, increased precipitation had a significant influence on pedogenic
452 intensity. Seasonal precipitation was intermittently enhanced from 4.7-3.9 Ma, and so was
453 weathering and pedogenic intensity. Pedogenesis and weathering intensity reached a
454 maximum during 4.60-4.25 Ma, as did precipitation intensity, manifested by the enhanced
455 eluviation and carbonate accumulation. Notably, during this interval of peak precipitation
456 (4.6-4.25 Ma), the enhancement of the $<2 \mu m$ / $>40 \mu m$ ratio is not as strong as that of χ_{pedo} ,
457 which may indicate that the former is of limited value when pedogenic intensity is strong.
458 During 3.9-3.6 Ma, precipitation decreased, and weathering and pedogenic intensity also
459 weakened. Consistent with the records of the XSZ section, mollusk records from Dongwan
460 also indicate the occurrence of warm and humid conditions in the western CLP during the

461 early Pliocene (Fig. 7 h).

462 Palynological and terrestrial mollusk records from the central CLP also indicate
463 relatively humid conditions during the early Pliocene (Wang et al., 2006; Wu et al., 2006).
464 Magnetic susceptibility records from the central and eastern CLP are similar to that from the
465 XSZ section in that both the magnitude and the variability are high during the early Pliocene.
466 From 4.1-3.9 Ma, the increased magnetic susceptibility indicates that humid climatic
467 conditions prevailed across the entire CLP (Fig. 7). Evidently, when precipitation amount
468 peaked in the vicinity of the XSZ section during 4.60-4.25 Ma, the magnetic susceptibility
469 values at Xifeng, Lingtai and Chaona were low. However, a record of Fe₂O₃ ratio from
470 Lingtai reveals extremely high values, corresponding to the presence of abundant clay
471 coatings, during 4.8-4.1 Ma and this interval was interpreted as experiencing the strongest
472 EASM intensity in the CLP since 7.0 Ma (Ding et al., 2001). In addition, the relative intensity
473 of pedogenic alteration of the grain-size distribution was the strongest during the interval
474 from 4.8-4.2 Ma in the Lingtai section (Sun et al., 2006c). Pollen assemblages at Chaona
475 indicate a substantially warmer and more humid climate from 4.61-4.07 Ma (Ma et al., 2005).
476 These various lines of evidence indicate that during 4.60-4.25 Ma the climate was warm and
477 humid in the central CLP. Gleying has been implicated in reducing the value of magnetic
478 susceptibility as a record of precipitation during this period (Ding et al., 2001). When soil
479 moisture regularly exceeds the critical value, dissolution of ferrimagnetic minerals occurs and
480 the susceptibility signal is negatively correlated with pedogenesis (Liu et al., 2003). This
481 alone indicates that precipitation was likely to have been very high during this interval.

482 In summary, a wet climate prevailed across the CLP in the early Pliocene. At the same

483 time, the hematite/goethite ratio in the sediments of the South China Sea also indicates
484 enhanced precipitation amount and the smectite/kaolinite ratio indicates increased seasonality
485 at ~4.7 Ma (Fig. 7 i and j) and thus the enhancement of the palaeo-EASM (Clift et al., 2006,
486 2014). Therefore, we regard the climatic change evident in XSZ section to reflect the
487 expansion of the palaeo-EASM.

~~488 The remarkably increased amplitude of the 41-kyr filtered components from the XSZ
489 section and the deep-sea $\delta^{18}\text{O}$ record at about 4.7 Ma indicates that the expansion of the
490 palaeo-EASM may have been related to changes in global temperature and ice volume.
491 Furthermore, a decrease in the input of ice-rafted debris to the sediments of the subarctic
492 northwest Pacific was synchronous with the expansion of the palaeo-EASM during the early
493 Pliocene (Fig. 6). In addition, from 4.8–4.7 Ma and 4.6–4.25 Ma, the high values of the three
494 pedogenic indices at the XSZ section indicate that strong pedogenic intensity corresponded
495 with high SSTs in the Eastern Equatorial Pacific (EEP). This coherence between the record of
496 the XSZ section and marine records implies that phases of enhanced precipitation were
497 correlative with changes in SST and ice volume (or temperature) at northern high latitudes.~~

498 **5.4 Possible driver of palaeo-EASM expansion during the early Pliocene**

499 Ding (2001) proposed that the uplift of the TP to a critical elevation resulted in an
500 enhanced summer monsoon system during 4.8–4.1 Ma. TP uplift was shown to have had
501 profound effects on the EASM in terms of its initiation and strength, as well as in changing
502 the distribution of the band of high precipitation in East Asia (Li et al., 1991, 2014; An et al.,
503 2001). A detailed modeling study demonstrated that the uplift of the northern TP mainly
504 resulted in an intensified summer monsoon and increased precipitation in northeast Asia

505 (Zhang et al., 2012). From 8.26-4.96 Ma, massive deltaic conglomerates were widely
506 deposited and the sediment deposition rate increased, indicating the uplift of the Qilian
507 Mountains (Song et al., 2001). At the same time, the Laji Mountains underwent pronounced
508 uplift by thrusting at ~8 Ma, which resulted in the current basin-range pattern (Li et al., 1991;
509 Fang et al., 2005a; Zheng et al., 2000). However, geological and palaeontological records
510 indicate that the uplift of the eastern and northern margins of the TP was very minor from the
511 late Miocene to the middle Pliocene (Li et al., 1991, 2015; Zheng et al., 2000; Fang et al.,
512 2005a, 2005b). Therefore, we speculate that uplift of the TP was not the major cause of the
513 expansion of the palaeo-EASM at ~4.7 Ma.

514
515 The occurrence of a humid climate across the CLP was synchronous with the gradual
516 closure of the Panama Seaway (Keigwin, 1978; O’Dea et al., 2016). Nie (2014) proposed that
517 the freshening of Eastern Equatorial and North Pacific surface water, resulting from the
518 closure of the Panama Seaway since 4.8 Ma (Haug et al., 2001), led to sea ice formation in
519 the North Pacific Ocean, which enhanced the high-pressure cell over the Pacific and
520 increased the strength of southerly and southeasterly winds. However, there was a warming
521 trend in the Northern Hemisphere from 4.6 Ma (Haug et al., 2005; Lawrence et al., 2006).
522 The gradual closure of the Panama Seaway resulted in the reorganization of surface currents
523 in the Atlantic Ocean. Notably, the Gulf Stream was enhanced and began to transport warm
524 surface waters to high northern latitudes, thus strengthening the Atlantic meridional
525 overturning circulation and warming the Arctic (Haug and Tiedemann, 1998; Haug et al.,
526 2005). Three independent proxies from an early Pliocene peat deposit in the Canadian High

527 Arctic indicate that Arctic temperatures were 19 °C warmer during the early Pliocene than
528 today ([Ballantyne et al., 2010](#)). This warmth is also confirmed by other records from high
529 northern latitude regions: diatom abundances and assemblages, pollen data, magnetic
530 susceptibility and sedimentological evidence from Siberia all indicate that the climate was
531 warm and wet in the early Pliocene ([Baikal Drilling Project Memb, 1997, 1999](#)). Furthermore,
532 a decrease in the input of ice-rafted debris to the sediments of the subarctic northwest Pacific
533 was synchronous with the expansion of the palaeo-EASM during the early Pliocene (Fig. 6).
534 ~~The warming of the northern high latitude region led to increases in summer temperature in~~
535 ~~the mid-latitudes of Eurasia. However, equatorial SSTs remained stable or cooled slightly~~
536 ~~([Brierley et al., 2009; Fedorov et al., 2013](#)), and thus the land-ocean thermal contrast was~~
537 ~~intensified. Furthermore, the warming of the Northern Hemisphere and~~ external heating
538 derived from a reduced ice albedo at high northern latitudes ~~also~~ enhanced the thermal
539 contrast between the Pacific and Eurasian regions ([Dowsett et al., 2010](#)). This large land-
540 ocean thermal contrast was essential for enhancing the palaeo-EASM. On the other hand, the
541 unusually warm high northern latitudes and the West Antarctic ice-sheet expansion by 6–5
542 Ma ([Zachos et al., 2001, 2008](#)) steepened interhemispheric thermal gradient and further
543 caused the thermal equator to move northward ([Chiang and Friedman, 2012; Broecker and](#)
544 [Putnam, 2013](#)). This facilitated the northwestward expansion of the palaeo-EASM, which is
545 also proposed as the driving mechanism for northwestward migration of the monsoon rain
546 belt for the warm Holocene ([Yang et al., 2015](#)).

547 ~~- small meridional heat gradient in the Northern Hemisphere pushed the Intertropical~~
548 ~~Convergence Zone northwards ([Chang et al., 2013; Sun et al., 2015](#)), which weakened the~~

549 ~~westerly circulation and thus facilitated the northwestward expansion of the palaeo-EASM.~~

550 ~~Figure 6 shows that high values of pedogenic indices in the XSZ section correspond~~
551 ~~with high SSTs in the EEP. This appears to be contradictory to the case of the modern ENSO~~
552 ~~(when the EEP temperature is high, the precipitation amount in the western CLP is low). The~~
553 ~~discrepancy may indicate that the nature of sea-air interactions during the early Pliocene was~~
554 ~~different from today. During 4.8–4.0 Ma, the thermohaline circulation was reorganizing and~~
555 ~~creating a precondition for the development of the modern equatorial Pacific cold tongue~~
556 ~~(Chaisson and Ravelo, 2000). Several crucial changes linked with the summer monsoon~~
557 ~~occurred: There was a vast expansion of the western Pacific warm pool into subtropical~~
558 ~~regions in the early Pliocene (Brierley et al., 2009; Fedorov et al., 2013), and temperatures at~~
559 ~~the edge of the warm pool showed a warming trend of ~ 2 °C from the latest Miocene to the~~
560 ~~early Pliocene (Karas et al., 2011). This enhanced thermal state of the WEP warm pool~~
561 ~~significantly enhanced the summer monsoon and its northward extension. A modelling~~
562 ~~experiment indicates that the precipitation of the CLP would increase when the tropical warm~~
563 ~~pool expended into subtropical region (Brierley et al., 2009). Today, when the northern part~~
564 ~~of the western Pacific warm pool is warm, convection over and around the Philippines is~~
565 ~~enhanced; in addition, the northern extent of the western Pacific subtropical high shifts~~
566 ~~northwards from the Yangtze River valley to the Yellow River valley and moisture is~~
567 ~~introduced across the entire CLP (Huang et al., 2003). Further research is needed to~~
568 ~~determine if this was also the case during the early Pliocene. However, the warming and~~
569 ~~freshening of the subtropical Pacific would have promoted increased evaporation which~~
570 ~~would have provided enhanced moisture for the palaeo-EASM, resulting in increased rainfall~~

571 ~~across the CLP.~~

572 ~~In conclusion, Therefore,~~ we infer that the warming of high northern latitudes in

573 response to the closure of the Panamanian Seaway, ~~accompanied by the vast poleward~~

574 ~~expansion of the tropical warm pool into subtropical regions and the freshening of the~~

575 ~~subtropical Pacific~~, may have facilitated the expansion of the palaeo-EASM during the early

576 Pliocene. However, there are several uncertainties associated with such an explanation. For

577 example, the timing of the closure of the Panama Seaway is still debated (Bacon et al., 2015;

578 O’Dea et al., 2016), and it is unclear how strongly these changes influenced the palaeo-

579 EASM. Addressing these questions requires more geological evidence and precise model

580 simulations of the early Pliocene climate. The value of our study lies in proposing the

581 potential linkage of the evolution of palaeo-EASM and changes in temperatures of high

582 northern latitudes during the early Pliocene and SSTs of the low latitude Pacific Ocean in the

583 early Pliocene.

584 **6. Conclusions**

585 The continuous late Miocene-Pliocene red clay sequence preserved on the planation

586 surface in the NE Tibetan Plateau provides the opportunity to elucidate the history of the

587 Asian monsoon in the western CLP. Multi-proxy records from the XSZ section, together with

588 other paleoclimatic records from the CLP, reveal the major patterns of climatic change from

589 6.7-3.6 Ma. During the late Miocene, both the amount and variability of precipitation over the

590 XSZ section were small; however, they were much greater in the central and eastern CLP;

591 thus, the palaeo-EASM had little influence on the climate of the western CLP at this time.

592 During the early Pliocene, the records from the XSZ section indicate that both the amount

593 and variability of precipitation increased from 4.7-3.9 Ma. The climate was characterized by
594 abrupt increases in the seasonality of precipitation, which attests to a major northwestward
595 extension and enhancement of the summer monsoon. Multiple paleoclimatic proxies clearly
596 show that the strongest summer monsoon occurred during 4.60-4.25 Ma. The expansion of
597 the palaeo-EASM may have been caused by warming of the ~~Aretic region~~high northern
598 latitudes, the vast poleward expansion of the tropical warm pool into subtropical regions, and
599 the freshening of the subtropical Pacific, in response to the closure of the Panamanian
600 Seaway during the early Pliocene.

601

602 **Acknowledgements**

603 We thank Ai Song, Jia Liu, Shanpin Liu and Jun Zhang for the drilling operation and
604 Fengxia Yu for her early experimental work. We thank Jan Bloemendal for modifying and
605 polishing the language. We specially thank Ran Feng and four anonymous reviewers for their
606 suggestions and comments that have helped improve the paper. This work was supported by
607 the National Natural Science Foundation of China (grants 41330745 and 41401214) and the
608 Key Laboratory of Continental Collision and Plateau Uplift, Institute of Tibetan Plateau
609 Research (LCP201602).

610

611 **References**

612 An, Z. S., Kutzbach, J. E., Prell, W. L., Porter, S. C.: Evolution of Asian monsoons and phased uplift of the

613 Himalayan Tibetan plateau since Late Miocene times. *Nature*, 411, 62–66, 2001.

614 An, Z. S.: *Late Cenozoic Climate Change in Asia*. Springer Netherlands, 2014.

615 Ao, H., Roberts, A. P., Dekkers, M. J., Liu, X., Rohling, E. J., Shi, Z., An, Z. S., and Zhao, X.: Late
616 Miocene–Pliocene Asian monsoon intensification linked to Antarctic ice-sheet growth. *Earth &*
617 *Planetary Science Letters*, 444, 75-87, 2016.

618 Avery, B. W., and Bascomb, C. L.: *Soil survey laboratory methods* /, 1974.

619 Bacon, C. D., Silvestro, D., Jaramillo, C., Smith, B. T., Chakrabarty, P., and Antonelli, A.: Biological
620 evidence supports an early and complex emergence of the Isthmus of Panama. *Proceedings of the*
621 *National Academy of Sciences*, 112(19), 6110-6115, 2015.

622 Ballantyne, A. P., Greenwood, D. R., Sinningh-Damste, J. S., Csank, A. Z., Eberle, J. J., and Rybczynski,
623 N.: Significantly warmer arctic surface temperatures during the Pliocene indicated by multiple
624 independent proxies. *Geology*, 38(7), 603-606, 2010.

625 Brierley, C. M., Fedorov, A. V., Liu, Z., Herbert, T. D., Lawrence, K. T., and Lariviere, J. P.: Greatly
626 expanded tropical warm pool and weakened Hadley circulation in the early Pliocene. *Science*,
627 323(5922), 1714-8, 2009.

628 Brierley, C. M., and Fedorov, A. V.: Relative importance of meridional and zonal sea surface temperature
629 gradients for the onset of the ice ages and Pliocene-pleistocene climate evolution. *Paleoceanography*,
630 25(4), 2010.

631 [Broecker, W.S., Putnam A.E.: Hydrologic impacts of past shifts of Earth's thermal equator offer insight](#)
632 [into those to be produced by fossil fuel CO₂. *Proc Natl Acad Sci USA* 110\(42\):16710–16715, 2013.](#)

633 Buggle, B., Glaser, B., Hambach, U., Gerasimenko, N., and Markovi, S.: An evaluation of geochemical
634 weathering indices in loess–paleosol studies. *Quaternary International*, 240(1–2):12-21, 2011.

635 [Chiang J. C. H., Friedman A. R.: Tropical cooling, interhemispheric thermal gradients, and tropical climate](#)
636 [change. *Annu Rev Earth Planet Sci* 40\(1\):383–412, 2012.](#)

637 ~~Chaisson, W. P., and Ravelo, A. C.: Pliocene development of the east-west hydrographic gradient in the~~
638 ~~equatorial Pacific. *Paleoceanography*, 15(5), 497-505, 2000.~~

639 Chang, H., An, Z. S., Wu, F. L., Jin, Z., Liu, W. G., and Song, Y. G.: A Rb/Sr record of the weathering
640 response to environmental changes in westerly winds across the tarim basin in the late Miocene to the
641 early Pleistocene. *Palaeogeography Palaeoclimatology Palaeoecology*, 386(6), 364-373, 2013.

642 Clift, P. D.: Controls on the erosion of cenozoic asia and the flux of clastic sediment to the ocean. *Earth &*
643 *Planetary Science Letters*, 241(3-4), 571-580, 2006.

644 Clift, P. D., Hodges, K. V., Heslop, D., Hannigan, R., Long, H. V., and Calves, G.: Correlation of
645 Himalayan exhumation rates and Asian monsoon intensity. *Nature Geoscience*, 1(12),
646 doi:10.1038/ngeo351, 2008.

647 Clift, P. D., Wan, S. M., and Blusztajn, J.: Reconstructing chemical weathering, physical erosion and
648 monsoon intensity since 25 Ma in the northern South China Sea: a review of competing
649 proxies. *Earth-Science Reviews*, 130(3), 86-102, 2014.

650 Compo, G., Whitaker, J., Sardeshmukh, P., and Mccoll, C.: The quality control system of the 20th century
651 reanalysis dataset. *Egu General Assembly*, 15, 2013.

652 Ding, Z. L., Yang, S. L., Sun, J. M., and Liu, T. S.: Iron geochemistry of loess and red clay deposits in the
653 Chinese loess plateau and implications for long-term Asian monsoon evolution in the last 7.0
654 ma. *Earth & Planetary Science Letters*, 185(1), 99-109, 2001.

655 Dowsett, H. J., Robinson, M., Haywood, A., Salzmann, U., Hill, D., Sohl, L. E., Chandler, M., Williams,
656 M., Foley, K., and Stoll, D. K.: The PRISM3D paleoenvironmental reconstruction. *Stratigraphy*, 7,
657 123-139, 2010.

658 Fedorov, A. V., Brierley, C. M., Lawrence, K. T., Liu, Z., Dekens, P. S., and Ravelo, A. C.: Patterns and

659 mechanisms of early Pliocene warmth. *Nature*, 496 (7443), 43, 2013.

660 Fang, X. M, Li, J. J, Derbyshire, E., Fitzpatrick, E. A., and Kemp, R. A.: Micromorphology of the Beiyuan
661 loess-paleosol sequence in Gansu province, China: geomorphological and paleoenvironmental
662 significance. *Palaeogeography Palaeoclimatology Palaeoecology*, 111(3–4), 289-303, 1994.

663 Fang, X. M., Ono, Y., Fukusawa, H., Pan, B. T., Li, J. J., Guan, D. H., Oi. K., Tsukamoto, S., Torii, M.,
664 and Mishima, T.: Asian summer monsoon instability during the past 60,000 years: magnetic
665 susceptibility and pedogenic evidence from the western Chinese Lloess plateau. *Earth & Planetary
666 Science Letters*, 168(3–4), 219-232, 1999.

667 Fang, X. M., Yan, M. D., Voo, R. V. D., Rea, D. K., Song, C. H., Parés, J. M., Gao J. P., Nie J. S., and Dai
668 S: Late Cenozoic deformation and uplift of the NE Tibetan plateau: evidence from high-resolution
669 magnetostratigraphy of the Guide basin, Qinghai province, China. *Geological Society of America
670 Bulletin*, 117(9), 1208-1225, 2005a.

671 Fang, X., Zhao, Z. J., Li J. J., Yan, M. D, Pan, B. T., Song, C. H., and Dai, S.: Magnetostratigraphy of the
672 late Cenozoic Laojunmiao anticline in the northern Qilian mountains and its implications for the
673 Northern Tibetan plateau uplift. *Science in China*, 48(7), 1040-1051, 2005b.

674 Fang, X. M, Wu, F. L., Hai, W. X., Wang, Y. D., Zhang, X. Z., and Zhang, W. L.: Plio-Pleistocene drying
675 process of Asian inland-sporopollen and salinity records from Yahu section in the central Qaidam
676 basin(in Chinese). *Quaternary Sciences* 28(5): 874-882, 2008.

677 Fedo, C. M., Nesbitt, H. W., and Young, G. M.: Unraveling the effects of potassium metasomatism in
678 sedimentary rocks and paleosols, with implications for paleoweathering conditions and
679 provenance. *Geology*, 23(10), 921-924, 1995.

680 Guo, Z. T., Peng, S. Z., Hao, Q. Z., Biscaye, P. E., and Liu, T. S.: Origin of the Miocene–Pliocene red-

681 earth formation at Xifeng in northern China and implications for paleoenvironments.
682 Palaeogeography Palaeoclimatology Palaeoecology, 170(1-2), 11-26, 2001.

683 Han, W., Fang, X., Berger, A., and Yin, Q.: An astronomically tuned 8.1 ma eolian record from the
684 Chinese Loess plateau and its implication on the evolution of Asian monsoon. Journal of Geophysical
685 Research Atmospheres, 116(D24114), 2011.

686 Haug, G. H., and Tiedemann, R.: Effect of the formation of the isthmus of Panama on Atlantic ocean
687 thermohaline circulation. Nature, 393(3), 673-676, 1998.

688 Haug, G. H., Tiedemann, R., Zahn, R., and Ravelo, A. C.: Role of Panama uplift on oceanic freshwater
689 balance. Geology, 29(3), 207-210, 2001.

690 Haug, G. H., Ganopolski, A., Sigman, D. M., Rosell-Mele, A., Swann, G. E., Tiedemann, R., Jaccard, S. L.,
691 Bollmann, B. J., Maslin, M. A., Leng, M. J., and Eglinton, G.: North pacific seasonality and the
692 glaciation of north America 2.7 million years ago. Nature, 433(7028), 821-825, 2005.

693 He, T., Chen, Y., Balsam, W., Qiang, X.K., Liu, L.W., Chen, J., Li, F.J.: Carbonate leaching processes in
694 the Red Clay Formation, Chinese Loess Plateau: Fingerprinting East Asian summer monsoon
695 variability during the late Miocene and Pliocene. Geophysical Research Letters, 40(1):194-198,
696 2013. Herbert, T. D., Peterson, and Liu, Z.: Tropical ocean temperatures over the past 3.5 million
697 years. Science, 328(5985), 1530-4, 2010.

698 Herbert, T. D., Lawrence, K. T., Tzanova, A., Peterson, L. C., Caballerogill, R., and Kelly, C. S.: Late
699 Miocene global cooling and the rise of modern ecosystems. Nature Geoscience, 9(11), 2016.

700 ~~Huang, R. H., Zhou L.T., and Chen, W.: The progresses of recent studies on the variabilities of the East~~
701 ~~Asian monsoon and their causes, Adv. Atmos. Sci., 20, 55-69, 2003.~~

702 Jansen, E., and Sjöholm, J.: Reconstruction of glaciation over the past 6 Myr from ice-borne deposits in the

703 Norwegian sea. *Nature*, 349(6310), 600-603, 1991.

704 ~~Karas, C., Nürnberg, D., Tiedemann, R., and Garbe-Schönberg, D. : Pliocene climate change of the~~
705 ~~southwest Pacific and the impact of ocean gateways. *Earth & Planetary Science Letters*, 301(1-2),~~
706 ~~117-124, 2011.~~

707 Keigwin, L. D.: Pliocene closing of the isthmus of Panama, based on biostratigraphic evidence from
708 nearby Pacific ocean and Caribbean sea cores. *Geology*, 6(10), 630, 1978.

709 King, T.: Quantifying non-linearity and geometry in time series of climate. *Quaternary Science Reviews*
710 15, 247-266, 1996.

711 Laskar, J.: Long-term solution for the insolation quantities of the earth. *Proceedings of the International*
712 *Astronomical Union*, 2(14), 101-106, 2004.

713 Lawrence, K. T., Liu, Z., and Herbert, T. D.: Evolution of the eastern tropical pacific through Plio-
714 Pleistocene glaciation. *Science*, 312(5770), 79-83, 2006.

715 Liang, L., Sun, Y., Beets, C. J., Prins, M. A., Wu, F., and Vandenberghe, J.: Impacts of grain size sorting
716 and chemical weathering on the geochemistry of Jingyuan loess in the northwestern Chinese Loess
717 plateau. *Journal of Asian Earth Sciences*, 69(12), 177-184, 2013.

718 Li, F. J., Rousseau, D. D., Wu, N., Hao, Q., and Pei, Y.: Late Neogene evolution of the East Asian
719 monsoon revealed by terrestrial mollusk record in western Chinese Loess plateau: from winter to
720 summer dominated sub-regime. *Earth & Planetary Science Letters*, 274(3-4), 439-447, 2008.

721 Li, J. J.: The environmental effects of the uplift of the Qinghai-Xizang plateau. *Quaternary Science*
722 *Reviews*, 10(6), 479-483, 1991.

723 Li, J. J., Fang, X., Song, C., Pan, B., Ma, Y., and Yan, M., Late Miocene-quaternary rapid stepwise uplift
724 of the ne Tibetan plateau and its effects on climatic and environmental changes. *Quaternary Research*,

725 81(3), 400-423, 2014.

726 Li, J. J., Zhou, S. Z., Zhao, Z. J., and Zhang, J.: The Qingzang movement: the major uplift of the Qinghai-
727 Tibetan plateau. *Science China Earth Sciences*, 58(11), 2113-2122, 2015.

728 Li, J. J., Ma, Z. H., Li, X. M., Peng, T. J., Guo, B. H., Zhang, J., Song, C. H., Liu, J. Hui, Z. C., Yu, H.,
729 Ye, X. Y., Liu, S. P., Wang, X. X.: Late Miocene-Pliocene geomorphological evolution of the
730 Xiaoshuizi peneplain in the Maxian Mountains and its tectonic significance for the northeastern
731 Tibetan Plateau. *Geomorphology*. 295 393-405, 2017.

732 Liu, X. M., Rolph, T., An, Z., and Hesse, P.: Paleoclimatic significance of magnetic properties on the red
733 clay underlying the loess and paleosols in China. *Palaeogeography Palaeoclimatology Palaeoecology*,
734 199(1), 153-166, 2003.

735 Liu, C. Q., Masuda, A., Okada, A., Yabuki, S., Zhang, J., and Fan, Z. L.: A geochemical study of loess and
736 desert sand in northern China: implications for continental crust weathering and composition.
737 *Chemical Geology*, 106 (3-4), 359-374, 1993.

738 Liu, Q., Jackson, M. J., Yu, Y., Chen, F., Deng, C., and Zhu, R.: Grain size distribution of pedogenic
739 magnetic particles in Chinese loess/paleosols. *Geophysical Research Letters*, 312(22), 359-393, 2004.

740 Liu, Q., Torrent, J., Maher, B. A., Yu, Y., Deng, C. L., Zhu, R., and Zhao X. X.: Quantifying grain size
741 distribution of pedogenic magnetic particles in Chinese loess and its significance for pedogenesis.
742 *Journal of Geophysical Research Atmosphere*, 110(B11), 2005.

743 Liu, W., Liu, Z., An, Z., Sun, J., Chang, H., Wang, N., and Dong, J. B.: Late Miocene episodic lakes in the
744 arid Tarim basin, western China. *Proceedings of the National Academy of Sciences*, 111(46), 16292-6,
745 2014.

746 Lu, H., Zhang, F., Liu, X., and Duce, R. A: Periodicities of palaeoclimatic variations recorded by loess-

747 paleosol sequences in China. *Quaternary Science Reviews*, 23(18–19), 1891–1900, 2004.

748 Ma, Y. Z., Wu, F. L., Fang, X. M., Li, J. J., An, Z. S., and Wei, W.: Pollen record from red clay sequence
749 in the central Loess plateau between 8.10 and 2.60 Ma. *Chinese Science Bulletin*, 50(19), 2234-2243,
750 2005. Baikal Drilling Project Memb.: Preliminary results of the first scientific drilling on lake Baikal,
751 Buguldeika site, southeastern Siberia. *Quaternary International*, 37(2), 3-17, 1997.

752 Baikal Drilling Project Memb.: Continuous paleoclimate record recovered for last 5 million years. *Eos*
753 *Transactions American Geophysical Union*, 78(51), 597-601, 1999.

754 Mudie, P. J., and Helgason, J.: Palynological evidence for Miocene climatic cooling in eastern iceland
755 about 9.8 myr ago. *Nature*, 303(5919), 689-692, 1983.

756 Nesbitt, H. W., Markovics, G., and Price, R. C.: Chemical processes affecting alkalis and alkaline earths
757 during continental weathering. *Geochimica Et Cosmochimica Acta*, 44(11), 1659-1666, 1980.

758 Nie, J. S., Stevens, T., Song, Y., King, J. W., Zhang, R., Ji, S. C, Gong L. S., and Cares, D.: Pacific
759 freshening drives Pliocene cooling and Asian monsoon intensification. *Scientific Reports*, 4, 5474,
760 2014.

761 O’Dea, A., Lessios H. A., Coates, A. G., Eytan, R. I., Restrepo-Moreno, S. A., Cione, A. L., Collins, L. S.,
762 Queiroz, A. D., Farris, D. W., Norris, R. D., Stallard, R. F., Woodburne, M. O., Aguilera, O., Aubry,
763 M. P., Berggren, W. A., Budd, A. F., Cozzuol, M. A., Coppard, S. E., Duque-Caro, H., Finnegan, S.,
764 Gasparini, G. M., Grossman, E. L., Johnson, K. G., Keigwin, L. D., Knowlton, N., Leigh, E. G.,
765 Leonard-Pingel, J. S., Marko, P. B., Pyenson, N. D., Rachello-Dolmen, P. G., Soibelzon, E.,
766 Soibelzon, L., Todd, J. A., Vermeij, G. J., and Jackson, J. B. C.: Formation of the Isthmus of Panama.
767 *Science Advances*, 2(8), 2016.

768 Pagani, M., Liu, Z., Lariviere, J., and Ravelo, A. C.: High earth-system climate sensitivity determined from

769 Pliocene carbon dioxide concentrations. *Nature Geoscience*, 3(1), 27-30, 2010.

770 Rossinsky V. J., and Swart, P. K.: Influence of climate on the formation and isotopic composition of
771 calcretes. In: Swart, P.K., Lohmann, K.C., McKenzie, J., Savin, S. (Eds.), *Climate Change in*
772 *Continental Isotopic Records*, American Geophysical Union: *Geophysical Monography*, 78, pp. 67-75,
773 1993.

774 Song, C. H., Fang, X. M., Li, J. J., Gao, J., Zhao, Z. J., and Fan, M. J.: Tectonic uplift and sedimentary
775 evolution of the Jiuxi basin in the northern margin of the Tibetan plateau since 13 Ma BP. *Science*
776 *China Earth Sciences*,44(1), 192-202, 2001.

777 Song, Y. G., Fang, X. M., Torii, M., Ishikawa, N., Li, J. J., and An, Z. S.: Late Neogene rock magnetic
778 record of climatic variation from Chinese eolian sediments related to uplift of the Tibetan
779 plateau. *Journal of Asian Earth Sciences*, 30(2), 324-332, 2007.

780 Sun, D. H., Bloemendal, J., Rea, D. K., An, Z. S., Vandenberghe, J.,and Lu, H., Su, R. X., and Liu, T.: .
781 Bimodal grain-size distribution of Chinese loess, and its palaeoclimatic implications. *Catena*, 55(3),
782 325-340, 2004.

783 Sun, J. M., and Liu, T. S. : The age of the Taklimakan desert. *Science*, 312 (5780), 1612-1621, 2006a.

784 Sun, J. M., and Huang, X.: Half-precessional cycles recorded in Chinese loess: response to low-latitude
785 insolation forcing during the last interglaciation. *Quaternary Science Reviews*, 25(9–10), 1065-1072,
786 2006b.

787 Sun, J. M., Liu, W. G., Liu, Z., Deng, T., Windley, B. F., and Fu, B.: Extreme aridification since the
788 beginning of the Pliocene in the Tarim basin, western China. *Palaeogeography Palaeoclimatology*
789 *Palaeoecology*, 2017.

790 Sun, Y. B., Lu, H. Y., and An, Z S.: Grain size of loess, palaeosol and red clay deposits on the Chinese
791 Loess plateau: significance for understanding pedogenic alteration and palaeomonsoon

792 evolution. *Palaeogeography Palaeoclimatology Palaeoecology*, 241(1), 129-138, 2006c.

793 Sun, Y. B., An, Z. S., Clemens, S. C., Bloemendal, J., and Vandenberghe, J.: Seven million years of wind
794 and precipitation variability on the Chinese Loess plateau. *Earth & Planetary Science Letters*, 297(3–
795 4), 525-535, 2010.

796 Sun, Y. B., Kutzbach, J., An, Z., Clemens, S., Liu, Z., Liu, W., Liu, X. D., Shi, Z. G., Zheng, W. P., Liang,
797 L., Yan, Y., and Li, Y.: Astronomical and glacial forcing of East Asian summer monsoon
798 variability. *Quaternary Science Reviews*, 115, 132-142, 2015.

799 Tripathi, A. K., Roberts, C. D., and Eagle, R. A.: Coupling of CO₂ and ice sheet stability over major climate
800 transitions of the last 20 million years. *Science*, 326(5958), 1394-1397, 2009.

801 Tang, H., Micheels, A., Eronen, J., and Fortelius, M.: Regional climate model experiments to investigate
802 the Asian monsoon in the late Miocene. *Climate of the Past*, 7(3), 847-868, 2011.

803 Vandenberghe, J., H. Lu, D. Sun, J. Huissteden, V., and Konert, M.: The late Miocene and Pliocene
804 climate in East Asia as recorded by grain size and magnetic susceptibility of the Red Clay deposits
805 (Chinese Loess Plateau), *Palaeogeography Palaeoclimatology Palaeoecology*, 204, 239–255,
806 doi:10.1016/S0031-0182(03)00729-6, 2004.

807 Wan, S. M., Tian, J., Steinke, S., Li, A., and Li, T.: Evolution and variability of the East Asian summer
808 monsoon during the Pliocene: evidence from clay mineral records of the South China
809 Sea. *Palaeogeography Palaeoclimatology Palaeoecology*, 293(1–2), 237-247, 2010.

810 Wang, H. B., Chen, F. H., and Zhang, J. W.: Environmental significance of grain size of loess-paleosol
811 sequence in western part of Chinese Loess plateau. *Journal of Desert Research*, 22(1), 21-26, 2002.

812 Wang, L., Lu, H. Y., Wu, N. Q., Li, J., Pei, Y. P., Tong, G. B., and Peng, S. Z.: Palynological evidence for
813 Late Miocene-Pliocene vegetation evolution recorded in the red clay sequence of the central Chinese

814 Loess Plateau and implication for palaeo-environmental change. *Palaeogeography Palaeoclimatology*
815 *Palaeoecology*. 241, 118–128, 2006.

816 Wara, M. W., Ravelo, A. C., and Delaney, M. L.: Permanent EI ni ño-like conditions during the Pliocene
817 warm period. *Science*, 309(5735), 758-61, 2005.

818 Watanabe, T., Suzuki, A., Minobe, S., Kawashima, T., Kameo, K., &Minoshima, K., Aguilar, Y. M., Wan,
819 R., Kawahata, H., Sowa, K., Nagai, T., and Kase, T.: Permanent EI ni ño during the Pliocene warm
820 period not supported by coral evidence. *Nature*, 471 (7337), 209-211, 2011.

821 Wu, N., Pei, Y., Lu, H., Guo, Z., Li, F., and Liu, T.: Marked ecological shifts during 6.2–2.4 ma revealed
822 by a terrestrial molluscan record from the chinese red clay formation and implication for
823 palaeoclimatic evolution. *Palaeogeography Palaeoclimatology Palaeoecology*, 233(3-4), 287-299,
824 2006.

825 Xia, D. S., Jia, J., Li, G., Zhao, S., Wei, H. T., and Chen, F. H.: Out-of-phase evolution between summer
826 and winter East Asian monsoons during the Holocene as recorded by Chinese Loess deposits.
827 *Quaternary Research*, 81(3), 500-507, 2014.

828 Yang, S. L., Ding, F., and Ding, Z. L.: Pleistocene chemical weathering history of Asian arid and semi-arid
829 regions recorded in loess deposits of China and Tajikistan. *Geochimica Et Cosmochimica Acta*, 70(7),
830 1695-1709, 2006.

831 [Yang, S. L., Ding, Z.L., Li, Y.Y., Wang, X., Jiang, W.Y., Huang, X.F.: Warming-induced northwestward](#)
832 [migration of the East Asian monsoon rain belt from the Last Glacial Maximum to the mid-Holocene.](#)
833 [Proc. Natl. Acad. Sci. USA 112, 13178–13183, 2015.](#)

834 Zachos, J., Pagani, M., Sloan, L., Thomas, E., and Billups, K.: Trends, rhythms, and aberrations in global
835 climate 65 Ma to present. *Science*, 292(5517), 686-93, 2001.

836 [Zachos, J.C., Dickens, G.R., Zeebe, R.E.: An early Cenozoic perspective on green-house warming and](#)
837 [carbon-cycle dynamics. Nature.451, 279–283, 2008.](#)

838 Zhang, R., Jiang, D. B., Liu, X. D., and Tian, Z. P.: Modeling the climate effects of different subregional
839 uplifts within the Himalaya-Tibetan plateau on Asian summer monsoon evolution. Science
840 Bulletin, 57(35), 4617-4626, 2012.

841 Zhang, Y. G., Pagani, M., and Liu, Z.: A 12-million-year temperature history of the tropical Pacific
842 ocean. Science, 344(6179), 84, 2014.

843 Zhao, J. B.: A study of the CaCO₃ illuvial horizons of paleosols and permeated pattern far rain water, J
844 Geogr Sci, 15(4), 344-350, 1995.

845 Zhao, J. B.: Illuvial CaCO₃ layers of paleosol in loess and its environmental significance, Journal of Xi'an
846 Engineering University, 20(3), 46-49, 1998.

847 Zheng, H. B, Mcaulay Powell, C., An, Z. S., Zhou, J., and Dong, G. R.: Pliocene uplift of the northern
848 Tibetan plateau. Geology, 28(8), 715, 2000.

849

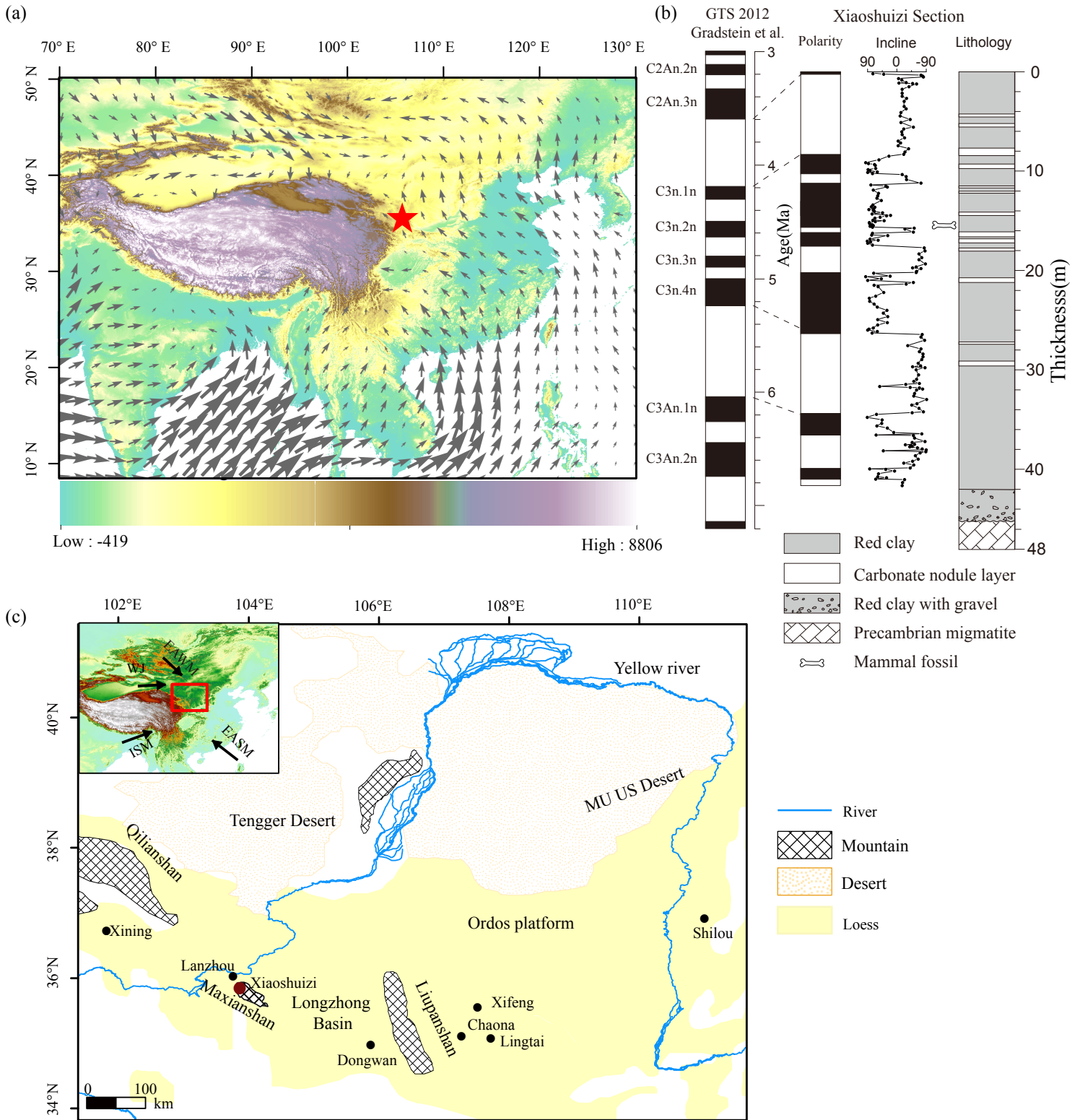


Fig. 1. Location of the study area and atmospheric circulation patterns. (a) 850 hPa vector wind averaged from June to August for 1982-2012 based on NOAA Earth System Research Laboratory reanalysis data (Compo et al., 2013). (b) Lithology and magnetostratigraphy of the XSZ drill core. (c) The Chinese Loess Plateau with locations of the studied Xiaoshuizi site and other sections mentioned in the text.



Fig. 2. Photos of the XSZ planation surface and the red clay. (a) XSZ planation surface.

(b) Red clay outcrop, XSZ. (c) Position of the XSZ drill hole. (d) The XSZ drill core.

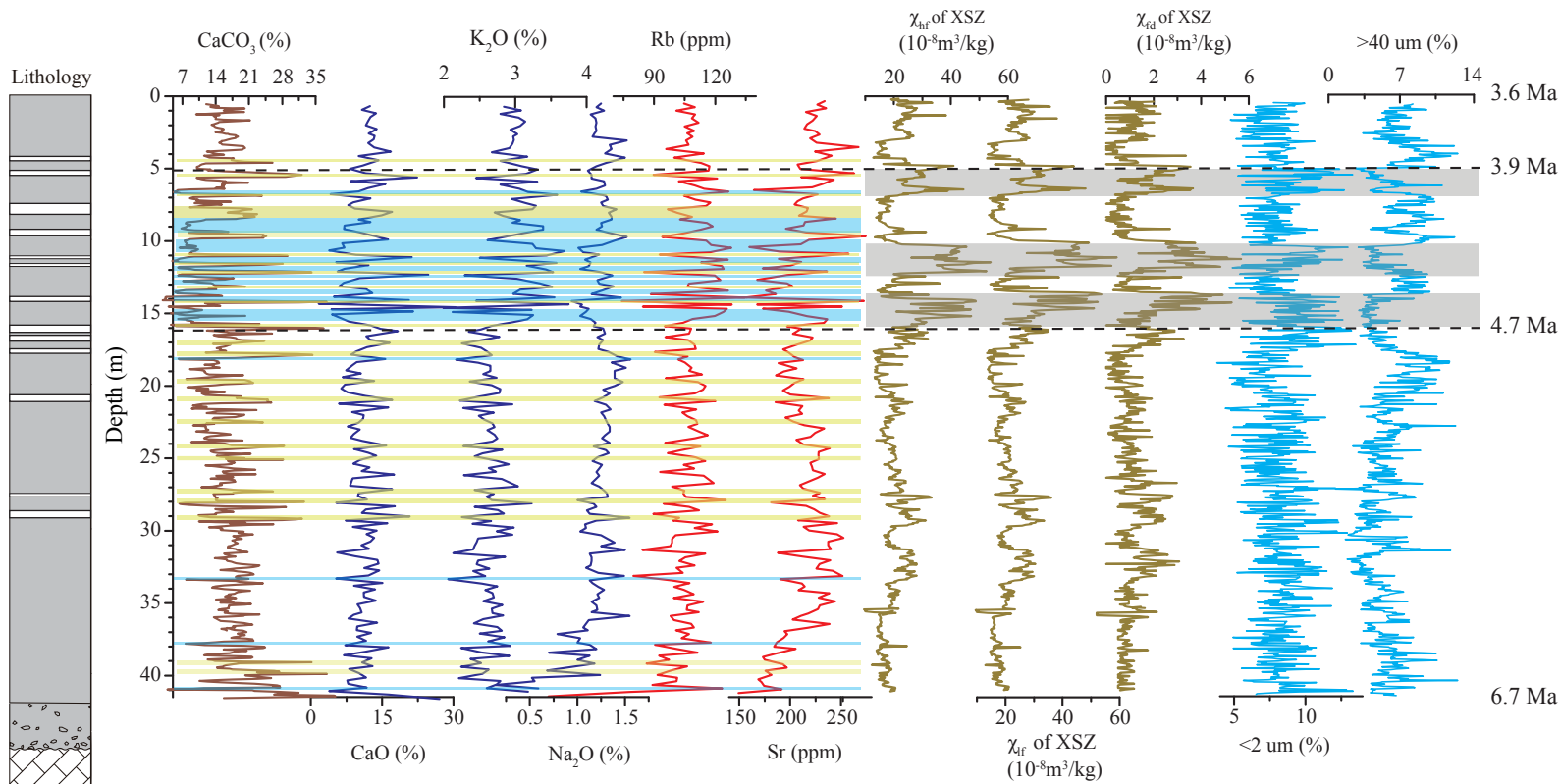


Fig. 3. Variations in carbonate content, major element concentration, minor element concentration, magnetic susceptibility and grain size for the XSZ red clay section (6.7-3.6 Ma). Yellow shading indicates Bk horizons with carbonate content >21%; blue shading indicates Bw horizons with carbonate content <8%; gray shading indicates intervals with high magnetic susceptibility. Dashed lines are upper and lower boundaries of the relatively wet interval.

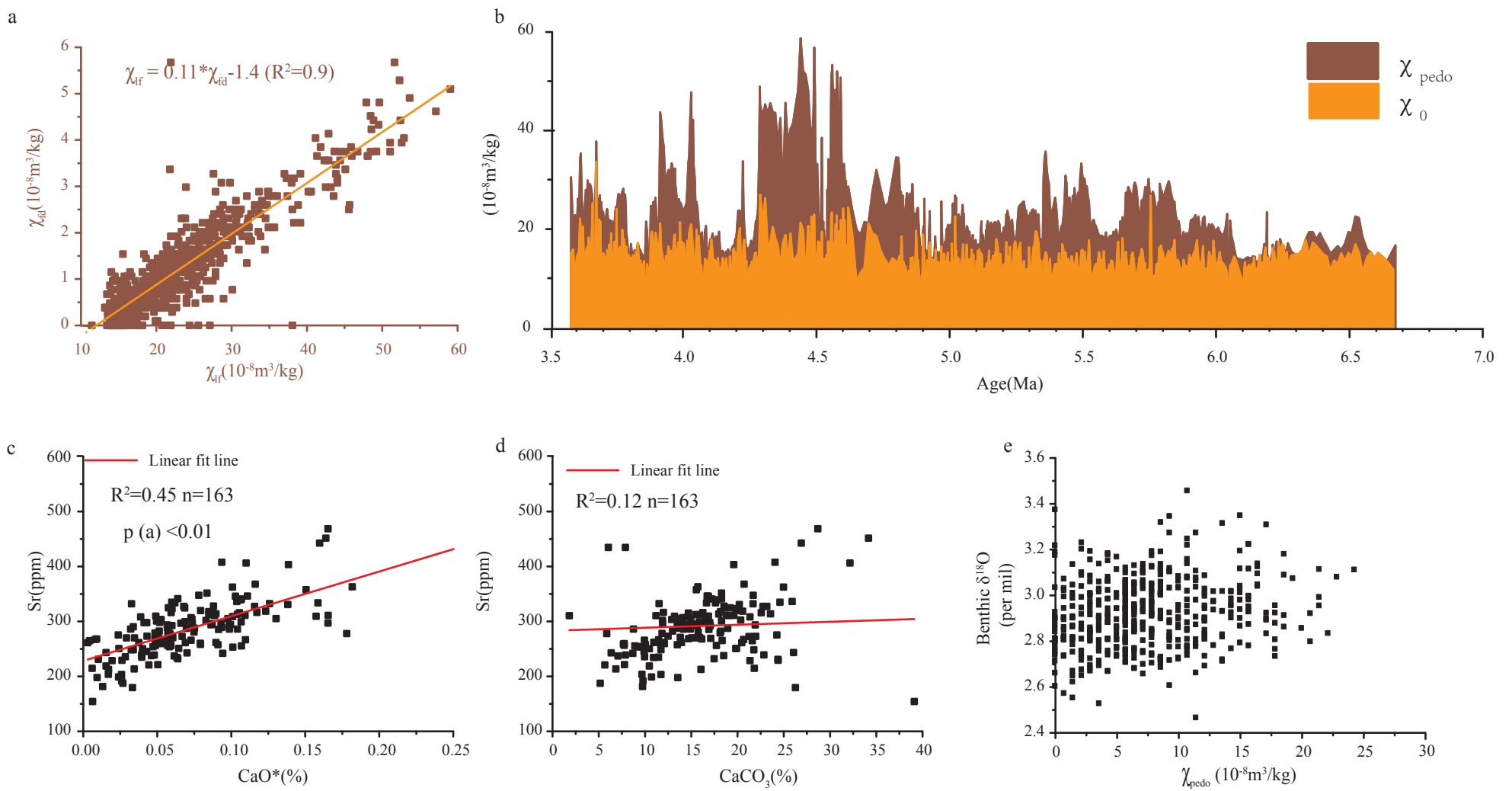


Fig. 4. (a) Scatter plot of χ_{if} versus χ_{fd} . (b) Separation of χ_{pedo} and χ_0 . (c) Scatter plot of Sr versus CaO*. (d) Scatter plot of Sr versus CaCO₃. (e) Scatter plot of benthic $\delta^{18}\text{O}$ versus χ_{pedo} during 6.7-5.2 Ma. χ_{pedo} is the magnetic susceptibility of pedogenic origin and χ_0 is the magnetic susceptibility of the detrital material.

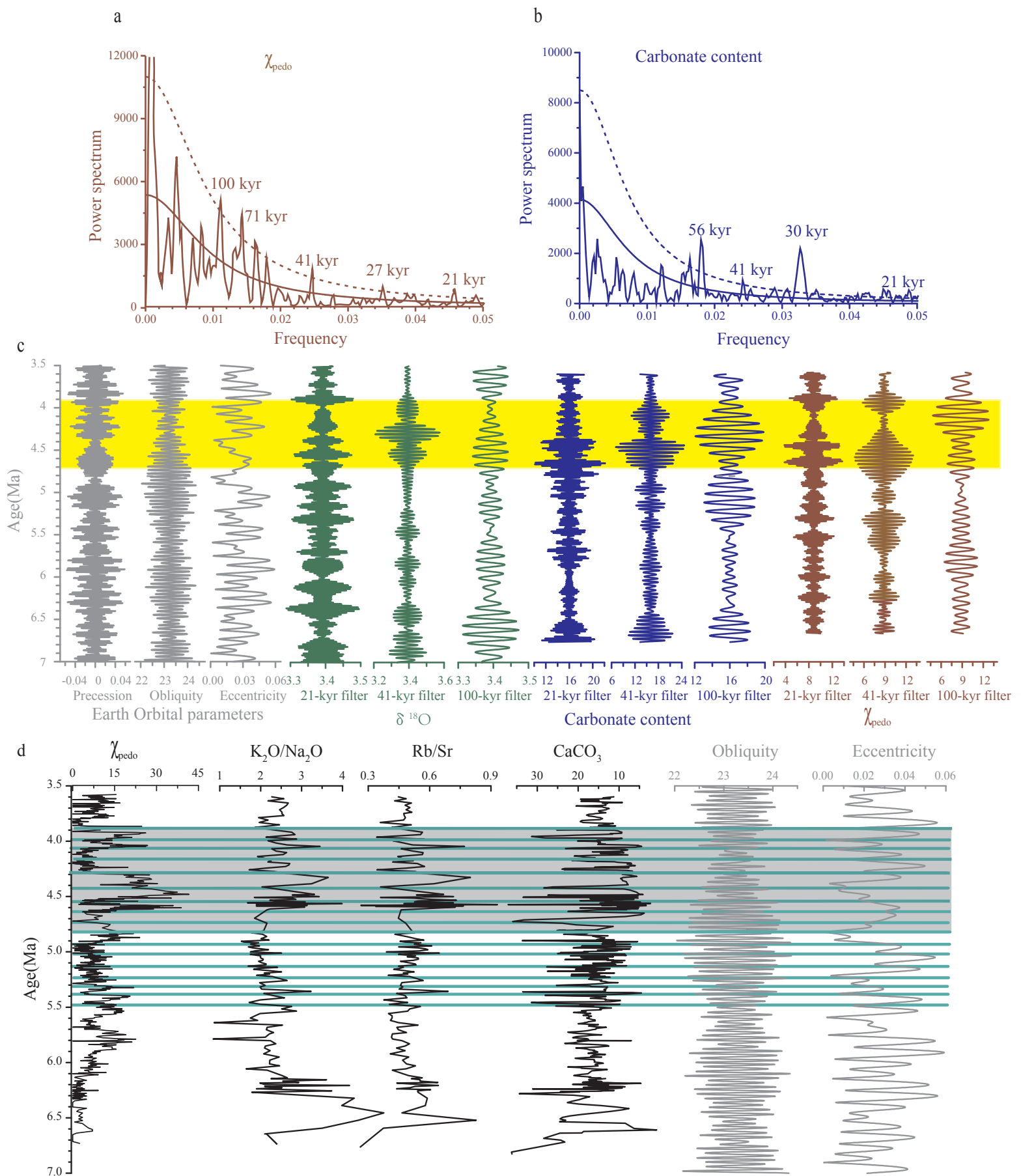


Fig. 5. Spectrum analysis results of the XSZ red clay section. (a) χ_{pedo} and (b) carbonate content (blue). (c) Comparison of orbital parameters (eccentricity, obliquity and precession - Laskar et al., 2004) with filtered components of the carbonate content, χ_{pedo} and $\delta^{18}\text{O}$ records (Zachos et al., 2001) in the 18–24 kyr, 36–46 kyr, and 90–110 kyr bands. Yellow shading denotes increased amplitude of the filtered components of carbonate and χ_{pedo} within the three orbital bands. (d) Carbonate, weathering and pedogenic indicators linked to eccentricity and obliquity orbital variations during 4.7–3.9 Ma.

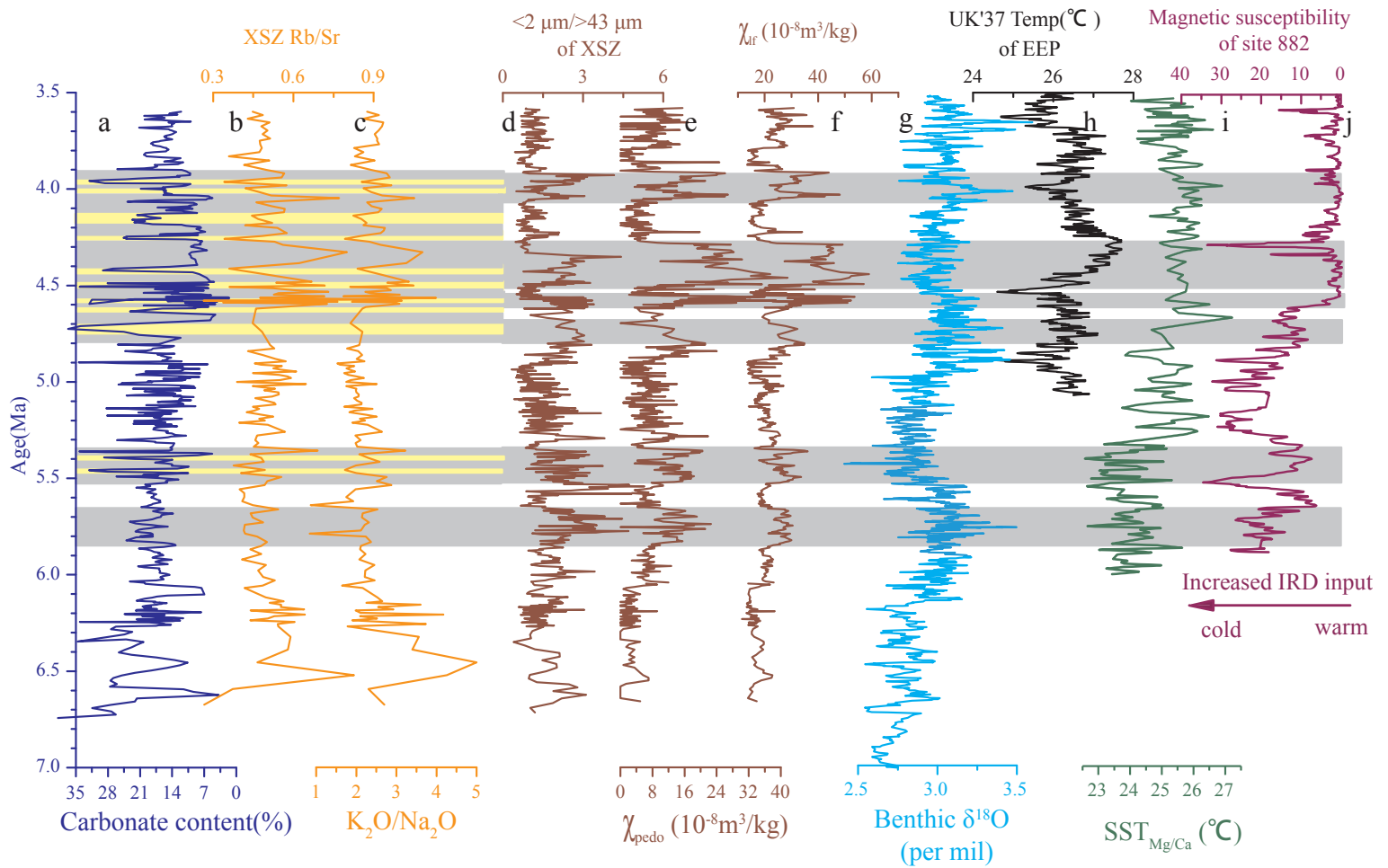


Fig. 6. Comparison of the paleoclimatic record of the XSZ red clay section with climate records from elsewhere.

(a) Effective precipitation record for the XSZ section; (b-c) chemical weathering records for the XSZ section; (d-f) pedogenic intensity records for the XSZ section; (g) stacked deep-sea benthic foraminiferal oxygen isotope curve compiled from data from DSDP and ODP sites (Zachos et al., 2001); (h) ~~reconstructed sea surface temperature in the eastern equatorial Pacific (EEP) from ODP Site 846 (Lawrence et al., 2006); (i) reconstructed temperature at the edge of the warm pool in the southwest Pacific Ocean, from ODP Site 590B (Karas et al., 2011); (j) magnetic susceptibility record from ODP Site 882 (Haug et al., 2005).~~ The gray shading indicates relatively wet periods and the light-yellow shading shows intervals of carbonate accumulation.

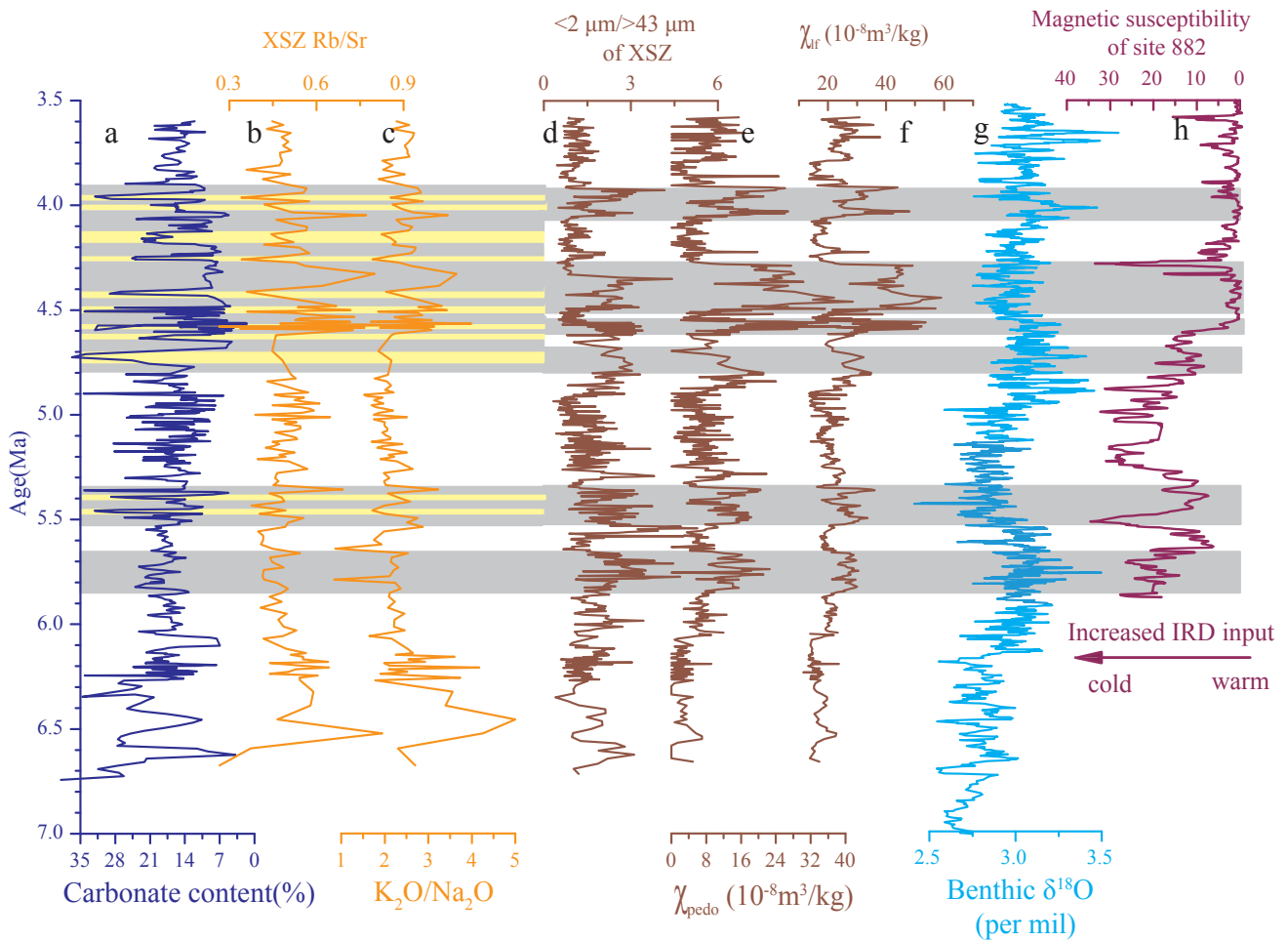


Fig. 6. Comparison of the paleoclimatic record of the XSZ red clay section with climate records from elsewhere. (a) Effective precipitation record for the XSZ section; (b-c) chemical weathering records for the XSZ section; (d-f) pedogenic intensity records for the XSZ section; (g) stacked deep-sea benthic foraminiferal oxygen isotope curve compiled from data from DSDP and ODP sites (Zachos et al., 2001); (h) magnetic susceptibility record from ODP Site 882 (Haug et al., 2005). The gray shading indicates relatively wet periods and the light-yellow shading shows intervals of carbonate accumulation.

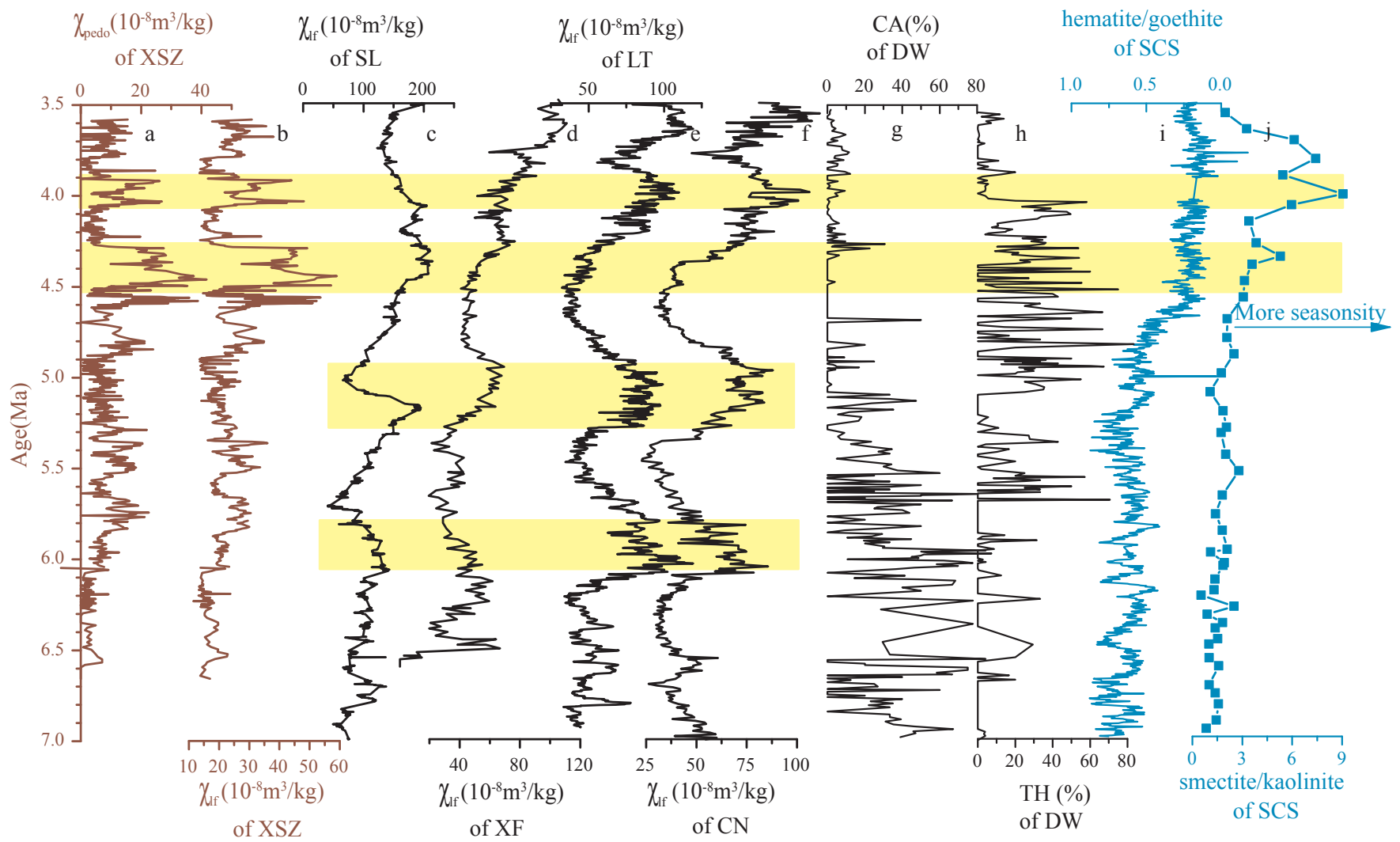


Fig. 7. Comparison of late Miocene-Pliocene paleoclimatic records from Asia. (a-b) χ_{pedo} and χ_{if} from the XSZ section. (c-f) χ_{if} record from Shilou (Ao et al., 2016), Xifeng (Guo et al., 2001), Lingtai (Sun et al., 2010) and Chaona (Song et al., 2007). (g-h) Percentages of cold-aridiphilous (CA) mollusks and thermo-humidiphilous (TH) mollusks from Dongwan (Li et al., 2008), (i) hematite/goethite ratio from sediments of the South China Sea (Clift, 2006), (j) smectite/kaolinite ratio from the South China Sea (Wan et al., 2010; Clift et al., 2014).

Table. 1. Average values and coefficients of variation of the geophysical and geochemical data for the

		XSZ section					
		CaCO ₃ (%)	CaO(%)	K ₂ O(%)	Na ₂ O(%)	Sr(ppm)	Rb(ppm)
3.9-3.6 Ma	Average	15.5	12.8	3.0	1.25	228.1	106.6
	CV	16.0	12.5	10.8	9.3	5.8	4.6
4.7-3.9 Ma	Average	13.3	11.2	3.1	1.21	210.4	111.0
	CV	53.6	45.3	13.8	10.5	14.0	12.1
6.7-4.7 Ma	Average	17.1	11.2	2.6	1.22	211.7	103.9
	CV	28.2	31.7	10.3	20.9	9.9	10.8
		χ_{hf}	χ_{lf}	χ_{fd}	χ_{pedo}	Rb/Sr	K ₂ O/Na ₂ O
3.9-3.6 Ma	Average	21.9	22.9	0.95	8.7	0.47	2.36
	CV	20.6	21.3	67.0	67.0	8.7	11.1
4.7-3.9 Ma	Average	27.4	29	1.6	14.5	0.55	2.58
	CV	36.2	37.8	78.9	78.9	25.0	20.9
6.7-4.7 Ma	Average	19.4	20.3	1.0	9.1	0.49	2.21
	CV	21.0	22.4	72.8	72.8	15.8	25.1

Table. 2. Correlation coefficients for geochemical data for the XSZ section

Pearson correlation	CaO	CaCO ₃	K ₂ O
CaO	1	0.51	-0.67
Na ₂ O	-0.06	-0.10	-0.38
K ₂ O	-0.67	-0.47	1
Rb	-0.20	-0.36	0.12
Sr	0.24	0.34	-0.29
CaCO ₃	0.51	1	-0.47

Table. 3. Results of a significance test for the correlations between CaO*, CaCO₃ and Sr

Pearson correlation	CaO*	CaCO ₃
Sr	0.67**	0.34
sig.(2-tailed)	0.000	0.063
n	163	163

**Correlation is significant at the 0.01 level